

A circuit mechanism for differentiating positive and negative associations

Praneeth Namburi^{1,2*}, Anna Beyeler^{1*}, Suzuko Yorozu³, Gwendolyn G. Calhoun¹, Sarah A. Halbert^{1,4}, Romy Wichmann¹, Stephanie S. Holden^{1,5}, Kim L. Mertens^{1,6}, Melodi Anahtar^{1,5}, Ada C. Felix-Ortiz^{1,2}, Ian R. Wickersham⁷, Jesse M. Gray³ & Kay M. Tye¹

The ability to differentiate stimuli predicting positive or negative outcomes is critical for survival, and perturbations of emotional processing underlie many psychiatric disease states. Synaptic plasticity in the basolateral amygdala complex (BLA) mediates the acquisition of associative memories, both positive^{1,2} and negative³⁻⁷. Different populations of BLA neurons may encode fearful or rewarding associations⁸⁻¹⁰, but the identifying features of these populations and the synaptic mechanisms of differentiating positive and negative emotional valence have remained unknown. Here we show that BLA neurons projecting to the nucleus accumbens (NAc projectors) or the centromedial amygdala (CeM projectors) undergo opposing synaptic changes following fear or reward conditioning. We find that photostimulation of NAc projectors supports positive reinforcement while photostimulation of CeM projectors mediates negative reinforcement. Photoinhibition of CeM projectors impairs fear conditioning and enhances reward conditioning. We characterize these functionally distinct neuronal populations by comparing their electrophysiological, morphological and genetic features. Overall, we provide a mechanistic explanation for the representation of positive and negative associations within the amygdala.

The BLA, including lateral and basal nuclei of the amygdala¹¹, receives sensory information from multiple modalities¹²⁻¹⁴, and encodes motivationally relevant stimuli¹⁵⁻¹⁷. Partially non-overlapping populations of BLA neurons encode cues associated with appetitive or aversive outcomes^{8,9}. The acquisition of the association between a neutral stimulus and an aversive outcome such as a foot shock has been shown to induce long term potentiation (LTP) of synapses onto lateral amygdala neurons^{3,4}, mediated by postsynaptic increases in α -amino-3-hydroxy-5-methyl-4-isoxazolepropionic acid receptor (AMPA)-mediated currents^{5,18} in a *N*-methyl-D-aspartate receptor (NMDAR)-dependent manner^{19,20}. Similarly, increases in glutamatergic synaptic strength of inputs to BLA neurons are necessary for the formation of a stimulus-reward association¹. Yet the similarity in neural encoding and synaptic changes induced by learning a positive or negative association and the contrasting nature of the ensuing outputs (reward-seeking or fear-related behaviours) presents an ostensible paradox: how is it possible that potentiation of synapses onto neurons in the BLA can underlie learned associations that lead to such different behavioural responses?

One hypothesis is that BLA neurons project to many downstream regions, including the canonical circuits for reward and fear^{14,30}, and the neurons that project to different targets undergo distinct synaptic changes with positive or negative associative learning. For example, BLA projections to the NAc have been implicated in reward-related behaviours^{16,21,22}, while BLA projections to the CeM have been linked to the expression of conditioned fear²³⁻²⁵. However, the unique syn-

aptic changes onto projection-identified BLA neurons have never been explored.

To investigate this, we selected the NAc and CeM as candidate target regions and examined the synaptic changes onto either NAc-projecting BLA neurons (NAc projectors) or CeM-projecting BLA neurons (CeM projectors) following fear conditioning or reward conditioning (Fig. 1). To identify the projection target of BLA neurons, we injected retrogradely travelling fluorescent beads (retrobeads) into either the NAc or CeM to label BLA neurons projecting axon terminals to these regions (Fig. 1a and Extended Data Fig. 1). After retrobead migration upstream to BLA cell bodies, we trained mice in fear or reward conditioning paradigms wherein a tone was paired with either a foot shock or sucrose delivery. Mice in reward conditioning groups were food restricted 1 day before the conditioning session to increase motivation to seek sucrose (Extended Data Fig. 1). AMPAR/NMDAR ratio, a proxy for glutamatergic synaptic strength, increases after either fear or reward conditioning in the BLA^{1,2,5,18}. We used matched experimental parameters across groups in an acute slice preparation stimulating axons arriving via the internal capsule and performing whole-cell patch-clamp recordings in retrobead-identified NAc projectors and CeM projectors, which we observed to be topographically intermingled (Fig. 1b and Extended Data Fig. 2).

We found that in NAc projectors, fear conditioning decreased the AMPAR/NMDAR ratio relative to controls exposed to the same number of tones and shocks, but where the tones and shocks were unpaired (Fig. 1c). Conversely, following the acquisition of the association between a tone and sucrose delivery, synapses on NAc projectors showed an increase in AMPAR/NMDAR ratio relative to unpaired controls that were also food restricted and received the same number of tones and volume of sucrose (Fig. 1d). Importantly, we also included naive and food-restricted naive groups (Fig. 1c-f), as food restriction itself could alter AMPAR/NMDAR ratio (Extended Data Fig. 3).

In contrast, synapses on CeM projectors from the paired group showed an increase in AMPAR/NMDAR ratio following fear conditioning, relative to unpaired controls (Fig. 1e). Following reward conditioning, CeM projectors from mice that learned the tone-sucrose association showed a decrease in AMPAR/NMDAR ratio relative to unpaired controls (Fig. 1f). In addition to AMPAR/NMDAR ratios, we also examined paired-pulse ratios, and did not detect any differences between groups (Extended Data Fig. 3), suggesting a postsynaptic mechanism of plasticity.

These results support a model wherein NAc and CeM projectors undergo opposing changes in synaptic strength following fear and reward learning, such that relative synaptic strengths onto CeM projectors increase following fear conditioning and decrease following reward learning. Conversely, relative synaptic strengths onto NAc

¹The Picower Institute for Learning and Memory, Department of Brain and Cognitive Sciences, Massachusetts Institute of Technology, Cambridge, Massachusetts 02139, USA. ²Neuroscience Graduate Program, Massachusetts Institute of Technology, Cambridge, Massachusetts 02139, USA. ³Department of Genetics, Harvard Medical School, 77 Avenue Louis Pasteur, NRB 356, Boston, Massachusetts 02115, USA. ⁴Undergraduate Program in Neuroscience, Wellesley College, Wellesley, Massachusetts 02481, USA. ⁵Undergraduate Program in Neuroscience, Massachusetts Institute of Technology, Cambridge, Massachusetts 02139, USA. ⁶Master's Program in Biomedical Sciences, University of Amsterdam, Amsterdam 1098 XH, The Netherlands. ⁷McGovern Institute for Brain Research, Massachusetts Institute of Technology, Cambridge, Massachusetts 02139, USA.

*These authors contributed equally to this work.

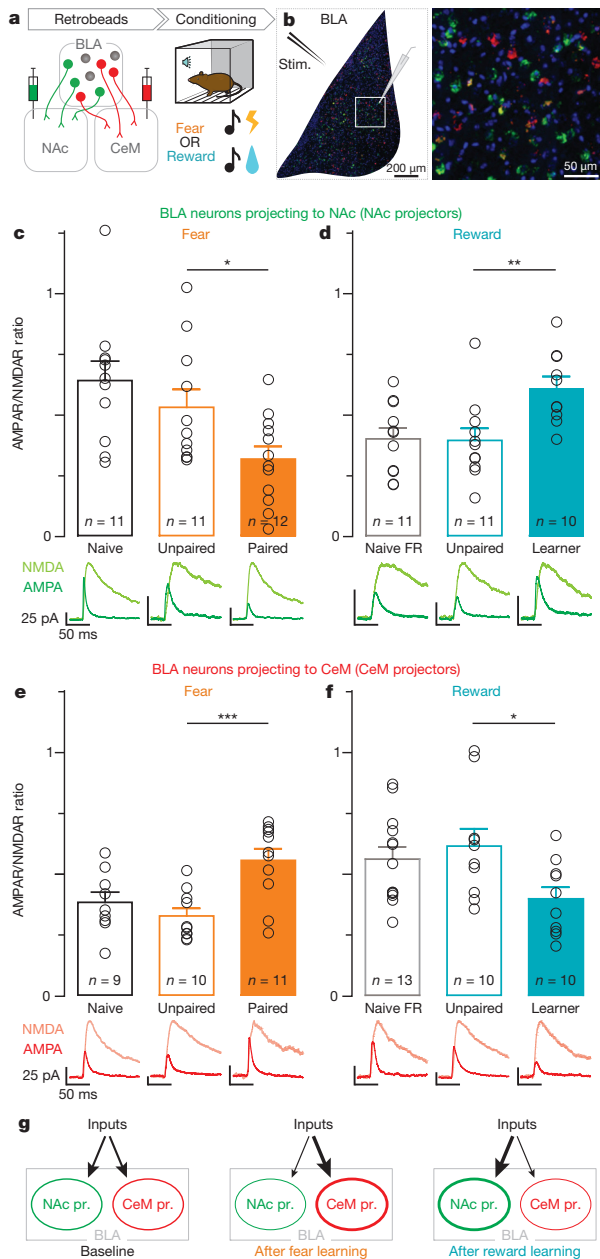


Figure 1 | Opposite changes in AMPAR/NMDAR following fear or reward conditioning in BLA neurons projecting to NAc or CeM. **a**, After injecting retrobeads into NAc or CeM, animals underwent either fear or reward conditioning. **b**, Confocal image of retrobead-labelled BLA neurons, with schematic of stimulation and recording sites (left); region in white square is enlarged (right). DAPI is shown in blue. **c–f**, One-way ANOVAs were performed on AMPAR/NMDAR ratios collected after conditioning. Open circles reflect individual data points, number of neurons are shown in each bar and representative traces for each group are below the bar. Results show mean and s.e.m. FR, food restricted. **c**, AMPAR/NMDAR ratio was related to training condition ($F_{2,33} = 5.844$, $P = 0.0070$) and significantly lower in the paired fear group relative to the unpaired fear group ($t_{31} = 2.21$, $*P < 0.05$). **d**, AMPAR/NMDAR ratio was related to training condition ($F_{2,31} = 6.53$, $P = 0.0046$) and reward learners showed a greater AMPAR/NMDAR ratio than mice in the unpaired reward group ($t_{29} = 3.20$, $**P < 0.01$). **e**, In CeM projectors, AMPAR/NMDAR ratio was related to fear conditioning ($F_{2,29} = 8.72$, $P = 0.0012$) and was greater in the paired group relative to the unpaired group ($t_{27} = 3.99$, $***P < 0.001$). **f**, In CeM projectors, AMPAR/NMDAR ratio was altered by reward learning ($F_{2,32} = 3.63$, $P = 0.039$), and was lower in learners relative to the unpaired group ($t_{30} = 2.57$, $*P < 0.05$). **g**, Proposed model, arrow thickness represents relative synaptic strength. CeM pr., CeM projectors; NAc pr., NAc projectors.

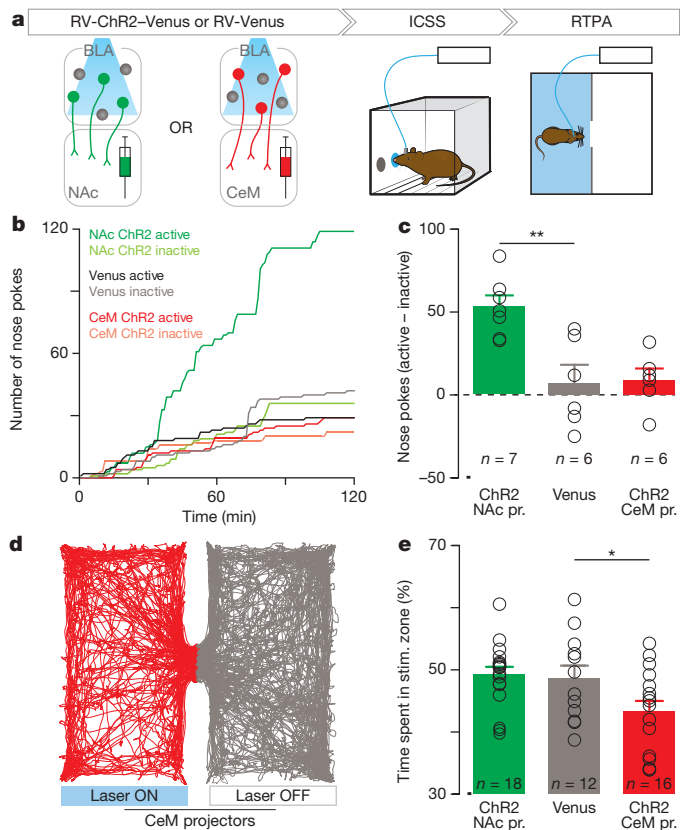


Figure 2 | Within the BLA, photostimulation of NAc or CeM projectors causes positive or negative reinforcement, respectively. **a**, After rabies virus injection into NAc or CeM, animals were tested using intracranial self-stimulation (ICSS) and real-time place avoidance (RTPA) assays. **b**, Representative traces of nose poke responses during ICSS. **c**, The relative number of active nose pokes was related to the experimental group (one-way ANOVA, $F_{2,18} = 10.50$, $P = 0.0012$), and was significantly increased by photostimulation of NAc projectors (NAc pr.) in comparison to controls ($t_{16} = 4.00$, $**P < 0.01$). CeM pr., CeM projectors. **d**, Representative locomotor trace from an animal receiving CeM projector photostimulation during RTPA. **e**, The percentage of time spent in the photostimulation-paired zone was related to the experimental group (one-way ANOVA, $F_{2,45} = 4.38$, $P = 0.019$) and was significantly decreased by photostimulation of CeM projectors in comparison to controls ($t_{43} = 2.25$, $*P < 0.05$). Results show mean and s.e.m.

projectors decrease following fear conditioning and increase following reward learning (Fig. 1g). However, these findings raise new questions. First, is there a causal relationship between the activity of BLA neurons projecting to the NAc and reward-related behaviours, and between the activity of CeM projectors and fearful or aversive behaviours? Second, what defining features of NAc and CeM projectors might endow them with their opposing functions?

To test whether there is a causal relationship between populations of projection-identified BLA neurons and behaviour, we first used a retrogradely infectious rabies viral (RV) vector²⁶ to express channelrhodopsin-2 (ChR2) fused to a fluorescent reporter (Venus), or a control virus carrying Venus alone (RV-Venus) in BLA neurons projecting to either the NAc or the CeM (Fig. 2a).

Following verification of functional ChR2 expression and retrograde transport from either the NAc or CeM back to the BLA (Extended Data Fig. 7), we tested animals receiving injections of RV-ChR2-Venus or RV-Venus into either the NAc or CeM and implantation of an optical fibre over the BLA on an intracranial self-stimulation (ICSS) task (Extended Data Fig. 4). Consistent with previous reports that photostimulation of BLA axons in the NAc produced ICSS²¹, we observed ICSS upon photostimulation of BLA cell bodies projecting to NAc (Fig. 2b, c). Given that we could not elicit robust nose-poke responses

for CeM projector photostimulation, we next tested CeM projectors in a closed-loop real-time place avoidance assay (RTPA), where an animal freely explored two chambers, one in which the mouse received photostimulation of CeM projectors. Photostimulation of CeM projectors caused robust avoidance of the light-paired side (Fig. 2d, e). Consistent with our data and previous studies, we demonstrated a causal relationship between NAc projectors and positive reinforcement and CeM projectors and negative reinforcement (avoidance).

We went on to probe the necessity of NAc or CeM projectors in mediating reward or fear conditioning. The acquisition of fear¹⁹ and reward¹ associations is mediated by an NMDAR-dependent LTP mechanism thought to require simultaneous glutamate release and postsynaptic depolarization. Thus, we tested whether projection-specific hyperpolarization during the presentation of the unconditioned stimulus could impair learning in a valence-specific manner.

To this end, we bilaterally infused an adeno-associated viral vector carrying halorhodopsin fused to an enhanced yellow fluorescent protein, or a no-opsin control (eYFP only), expressed in a Cre-dependent manner (double-floxed inverted open reading frame) into the BLA (Extended Data Fig. 5). We then bilaterally infused a retrogradely travelling canine adenovirus carrying Cre recombinase (CAV-Cre) into either the NAc or CeM (Fig. 3a). We illuminated the BLA with yellow light only during conditioned–unconditioned stimulus pairing, that is, during shock or sucrose consumption. Photoinhibition of CeM projectors during the conditioned–unconditioned stimulus pairing impaired conditioned freezing (Fig. 3b and Extended Data Fig. 6) and enhanced conditioned reward seeking (Fig. 3c).

Next, because there was no topographical separation between NAc and CeM projectors (Fig. 1b), which are both glutamatergic^{11,21,27,28}, we searched for distinguishing characteristics of these functionally distinct neuronal populations. As the BLA is known to have some heterogeneity

in electrophysiological and morphological characteristics^{11,29}, we compared these features between NAc and CeM projectors. While we did not observe differences in action potential half-width (Fig. 4a, b), threshold to spike (Fig. 4c, d), or intrinsic excitability (Fig. 4e, f), we did observe a significant difference in action potential accommodation (Fig. 4g and Extended Data Fig. 7). To investigate the morphological

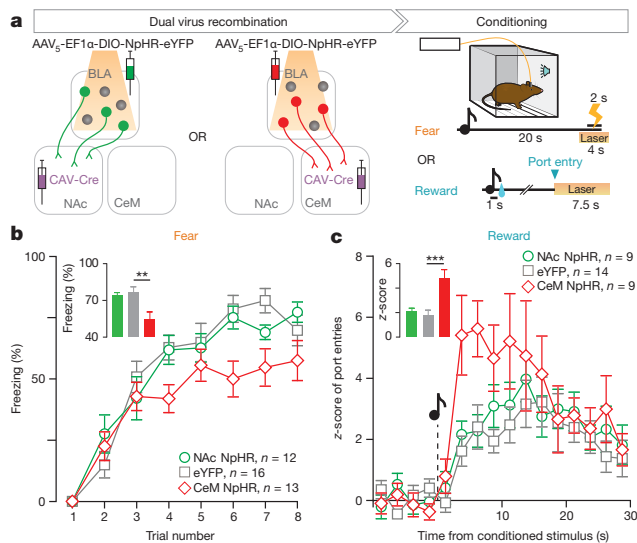


Figure 3 | Photoinhibition of CeM projectors impairs fear learning and enhances reward learning. **a**, Halorhodopsin (NpHR) was expressed bilaterally either in NAc- or CeM-projecting BLA neurons using a dual-virus recombination strategy. Mice underwent fear or reward conditioning and yellow light was delivered to the BLA during each unconditioned stimulus. **b**, Time course of percentage freezing and average freezing in trials 6–8 (inset). Average freezing was related to experimental condition (one-way ANOVA, $F_{2,40} = 6.68$, $P = 0.0033$) and was significantly reduced by photoinhibition of CeM projectors, relative to controls ($t_{38} = 3.46$, $**P < 0.01$; see inset). **c**, Time course of normalized number of port entries relative to cue presentation during reward conditioning and average number of normalized port entries (< 8 s latency, inset). z-score of port entries was related to the experimental condition (one-way ANOVA, $F_{2,31} = 9.23$, $P = 0.0008$) and was significantly increased by photoinhibition of CeM projectors, relative to controls ($t_{29} = 4.11$, $***P < 0.001$). Results show mean and s.e.m.

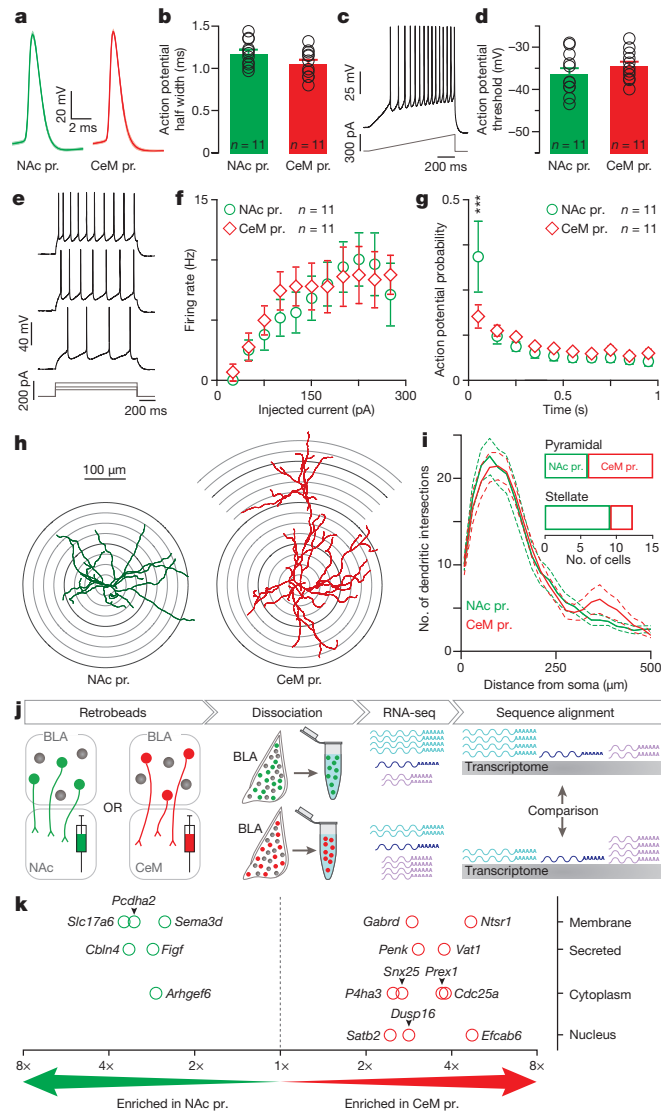


Figure 4 | Electrophysiological, morphological and transcriptional profiles of NAc and CeM projectors. **a**, Population average of action potential traces. CeM pr., CeM projectors; NAc pr., NAc projectors. **b**, No detectable difference in action potential half-width (unpaired t -test, $t_{20} = 1.82$, $P = 0.085$). Open circles represent individual data points. **c**, Representative trace from action potential threshold detection protocol. **d**, No detectable difference in action potential threshold between NAc and CeM projectors (unpaired t -test, $t_{20} = 1.05$, $P = 0.31$). **e–g**, Representative trace (**e**) from current injection protocol to determine firing rate responses (**f**) and action potential probability (**g**) over time, which was different between NAc and CeM projectors (interaction, two-way ANOVA $F_{9,180} = 2.32$, $P = 0.017$) in the first 100 ms of current injection ($t_{200} = 4.55$, $***P < 0.001$). **h**, Representative reconstructions showing dendritic branching pattern in the coronal plane. Cells were classified into pyramidal or stellate based on the presence of an apical tuft (right). **i**, Sholl analysis of neuron reconstructions. **j**, Schematic of transcriptome profiling. **k**, Candidate genes identified as differentially expressed between NAc and CeM projectors at a 0.01 quantile fold-change threshold, corresponding to a false discovery rate (FDR) of 26.2% (see also Extended Data Fig. 9) across two independent repetitions of RNA-seq ($n=8$ mice for NAc pr., $n=9$ mice for CeM pr. total). Results show mean and s.e.m.

features of these functionally distinct populations, we reconstructed projection-identified BLA neurons. We observed greater distal dendritic branching in CeM projectors (Fig. 4h, i), though NAc projectors and CeM projectors contained both pyramidal and stellate cells (Fig. 4i inset and Extended Data Fig. 8).

Finally, we compared the transcriptomes of BLA neurons projecting to the NAc or CeM (Fig. 4j and Extended Data Fig. 9). Following retrobead injections into the NAc or CeM, we dissociated labelled BLA neurons and performed RNA-seq (Fig. 4j). RNA-seq revealed relatively few candidate genes expressed differentially between NAc and CeM projectors, consistent with the idea that these two populations are closely related (Fig. 4k and Extended Data Fig. 9). However, these differentially expressed candidate genes may underpin the mechanisms that contribute to the wiring of these distinct populations through development and/or rapidly biasing gain modulation of synaptic transmission during valence-specific learning.

Taken together, NAc and CeM projectors are populations of BLA neurons that undergo opposing synaptic changes following fear or reward conditioning, and optogenetic manipulation of NAc and CeM projectors reveals causal relationships with valence-specific behaviours. Further, we have identified distinguishing electrophysiological, morphological and gene expression characteristics that facilitate further investigation. Our study suggests that the indelible nature of valence encoding observed in amygdala neurons¹⁰ is mediated by connectivity, and the topographical intermingling of these populations may serve to facilitate interaction³⁰. In conclusion, the BLA is a site of divergence for circuits mediating positive and negative emotional or motivational valence.

Online Content Methods, along with any additional Extended Data display items and Source Data, are available in the online version of the paper; references unique to these sections appear only in the online paper.

Received 13 April 2014; accepted 3 March 2015.

1. Tye, K. M., Stuber, G. D., De Ridder, B., Bonci, A. & Janak, P. H. Rapid strengthening of thalamo-amygdala synapses mediates cue-reward learning. *Nature* **453**, 1253–1257 (2008).
2. Tye, K. M. *et al.* Methylphenidate facilitates learning-induced amygdala plasticity. *Nature Neurosci.* **13**, 475–481 (2010).
3. McKernan, M. G. & Shinnick-Gallagher, P. Fear conditioning induces a lasting potentiation of synaptic currents *in vitro*. *Nature* **390**, 607–611 (1997).
4. Rogan, M. T., Stäubli, U. V. & LeDoux, J. E. Fear conditioning induces associative long-term potentiation in the amygdala. *Nature* **390**, 604–607 (1997).
5. Rumpel, S., LeDoux, J., Zador, A. & Malinow, R. Postsynaptic Receptor Trafficking Underlying a Form of Associative Learning. *Science* **308**, 83–88 (2005).
6. Maren, S. Synaptic mechanisms of associative memory in the amygdala. *Neuron* **47**, 783–786 (2005).
7. Han, J.-H. *et al.* Selective erasure of a fear memory. *Science* **323**, 1492–1496 (2009).
8. Paton, J. J., Belova, M. A., Morrison, S. E. & Salzman, C. D. The primate amygdala represents the positive and negative value of visual stimuli during learning. *Nature* **439**, 865–870 (2006).
9. Shabel, S. J. & Janak, P. H. Substantial similarity in amygdala neuronal activity during conditioned appetitive and aversive emotional arousal. *Proc. Natl Acad. Sci. USA* **106**, 15031–15036 (2009).
10. Redondo, R. L. *et al.* Bidirectional switch of the valence associated with a hippocampal contextual memory engram. *Nature* **513**, 426–430 (2014).
11. Sah, P., Faber, E. S. L., Lopez De Armentia, M. & Power, J. The amygdaloid complex: anatomy and physiology. *Physiol. Rev.* **83**, 803–834 (2003).
12. Romanski, L. M., Clugnet, M.-C., Bordi, F. & LeDoux, J. E. Somatosensory and auditory convergence in the lateral nucleus of the amygdala. *Behav. Neurosci.* **107**, 444–450 (1993).
13. Fontanini, A., Grossman, S. E., Figueroa, J. A. & Katz, D. B. Distinct subtypes of basolateral amygdala taste neurons reflect palatability and reward. *J. Neurosci.* **29**, 2486–2495 (2009).
14. Pitkänen, A. in *The Amygdala: A Functional Analysis* 2nd edn (ed. Aggleton, J. P.) Ch. 2 (Oxford Univ. Press, 2000).
15. Davis, M. The role of the amygdala in fear and anxiety. *Annu. Rev. Neurosci.* **15**, 353–375 (1992).
16. Cardinal, R. N., Parkinson, J. A., Hall, J. & Everitt, B. J. Emotion and motivation: the role of the amygdala, ventral striatum, and prefrontal cortex. *Neurosci. Biobehav. Rev.* **26**, 321–352 (2002).
17. Uwano, T., Nishijo, H., Ono, T. & Tamura, R. Neuronal responsiveness to various sensory stimuli, and associative learning in the rat amygdala. *Neuroscience* **68**, 339–361 (1995).
18. Clem, R. L. & Huganir, R. L. Calcium-permeable AMPA receptor dynamics mediate fear memory erasure. *Science* **330**, 1108–1112 (2010).
19. Miserendino, M. J. D., Sananes, C. B., Melia, K. R. & Davis, M. Blocking of acquisition but not expression of conditioned fear-potentiated startle by NMDA antagonists in the amygdala. *Nature* **345**, 716–718 (1990).
20. Fanselow, M. S. & LeDoux, J. E. and others. Why we think plasticity underlying Pavlovian fear conditioning occurs in the basolateral amygdala. *Neuron* **23**, 229–232 (1999).
21. Stuber, G. D. *et al.* Excitatory transmission from the amygdala to nucleus accumbens facilitates reward seeking. *Nature* **475**, 377–380 (2011).
22. Ambroggi, F., Ishikawa, A., Fields, H. L. & Nicola, S. M. Basolateral amygdala neurons facilitate reward-seeking behavior by exciting nucleus accumbens neurons. *Neuron* **59**, 648–661 (2008).
23. Jimenez, S. A. & Maren, S. Nuclear disconnection within the amygdala reveals a direct pathway to fear. *Learn. Mem.* **16**, 766–768 (2009).
24. Haubensak, W. *et al.* Genetic dissection of an amygdala microcircuit that gates conditioned fear. *Nature* **468**, 270–276 (2010).
25. Ciochi, S. *et al.* Encoding of conditioned fear in central amygdala inhibitory circuits. *Nature* **468**, 277–282 (2010).
26. Wickersham, I. R. *et al.* Monosynaptic restriction of transsynaptic tracing from single, genetically targeted neurons. *Neuron* **53**, 639–647 (2007).
27. Paré, D., Smith, Y. & Paré, J.-F. Intra-amygdaloid projections of the basolateral and basomedial nuclei in the cat: *Phaseolus vulgaris*-leucoagglutinin anterograde tracing at the light and electron microscopic level. *Neuroscience* **69**, 567–583 (1995).
28. Tye, K. M. *et al.* Amygdala circuitry mediating reversible and bidirectional control of anxiety. *Nature* **471**, 358–362 (2011).
29. Washburn, M. S. & Moises, H. C. Electrophysiological and morphological properties of rat basolateral amygdaloid neurons *in vitro*. *J. Neurosci.* **12**, 4066–4079 (1992).
30. Janak, P. H. & Tye, K. M. From circuits to behaviour in the amygdala. *Nature* **517**, 284–292 (2015).

Acknowledgements We thank C. Wildes, G. Glocker, R. Luck and G. F. Conyers for technical assistance. We thank the entire Tye laboratory, B. Okaty, U. Eser, J. di Iulio and A. Pfennig for helpful discussion. We thank E. J. Kremer for providing the CAV2-Cre virus, R. Neve for the HSV virus carrying Cre recombinase and mCherry, and the UNC vector core for the AAV viruses carrying double floxed constructs. K.M.T. is a New York Stem Cell Foundation–Robertson Investigator and holds a Whitehead Career Development Chair. This work was supported by funds from NIMH (R01-MH102441-01), NIDDK (DP2-DK-102256-01), the JPB Foundation (PIIF and PNDRF), NARSAD, Klingenstein, Whitehall and Sloan Foundations (K.M.T.). Additionally, S.Y. and J.G. were supported by NIMH (R01-MH101528-01), P.N. was supported by Singleton, Leventhal and Whitaker fellowships, and A.B. was supported by a fellowship from the Swiss National Science Foundation. R.W. was supported by post-doctoral fellowships from the Simons Center for the Social Brain and the Netherlands Organization for Scientific Research (NWO) RUBICON fellowship program. I.R.W. was supported by seed grants from the McGovern Institute for Brain Research, the Picower Institute for Learning and Memory, the MIT Department of Brain and Cognitive Sciences, and the Simons Center for the Social Brain, as well as by BRAIN Initiative awards from NIMH, NEI, and NINDS (U01-MH106018 and U01-NS090473) and NSF (IOS-1451202).

Author Contributions K.M.T. supervised all experiments. P.N., A.B. and K.M.T. designed the experiments. P.N., A.B., G.G.C., S.Y., R.W., S.S.H., M.A., S.A.H., and K.L.M. collected data. P.N., S.S.H., A.C.F.-O. and K.L.M. reconstructed neurons. P.N. wrote all MATLAB scripts. S.Y. and J.G. contributed to RNA-seq experiments and analyses. P.N., A.B. and G.G.C. analysed all other data sets. I.R.W. designed and provided rabies viral vectors. K.M.T., P.N., A.B. and G.G.C. wrote the manuscript and all authors read and edited the manuscript.

Author Information RNA-seq data has been deposited in the NCBI Gene Expression Omnibus (GEO) under accession code GSE66345. Reprints and permissions information is available at www.nature.com/reprints. The authors declare no competing financial interests. Readers are welcome to comment on the online version of the paper. Correspondence and requests for materials should be addressed to K.M.T. (kaytye@mit.edu)

METHODS

Animals and stereotaxic surgery. Adult wild-type male C57BL/6 mice (248 mice), aged 6–12 weeks (8.3 ± 1.5 weeks; Jackson Laboratory or Charles River Laboratories for RNA-seq) were used for experiments. Following surgery, animals were maintained on a reverse 12 h light/dark cycle with *ad libitum* food and water. All procedures of handling animals were in accordance with the guidelines from the NIH, and with approval of the MIT or Harvard Medical School Institutional Animal Care and Use Committee. All surgeries were conducted under aseptic conditions using a digital small animal stereotaxic instrument (David Kopf Instruments).

Mice were anaesthetized with isoflurane (5% for induction, 1.5–2.0% afterward) in the stereotaxic frame for the entire surgery and their body temperature was maintained with a heating pad. In order to label basolateral amygdala (BLA) neurons projecting to the nucleus accumbens (NAc), about 70 nl of red or green retrobeads (RetroBeads, Lumafluor Inc.) were injected into the NAc at stereotaxic coordinates from bregma: +1.4 mm anteroposterior, ± 0.87 mm mediolateral and -4.7 mm dorsoventral. In order to label BLA neurons projecting to the medial part of the central amygdala (CeM), 50 nl of retrobeads (different colour from NAc injection) were injected in the contralateral CeM (-0.75 mm anteroposterior, ± 2.35 mm mediolateral and -5.08 mm dorsoventral). To test the causal role of BLA neurons projecting to NAc or to CeM in reward and aversive behaviours, we injected a retrogradely travelling rabies virus carrying channelrhodopsin2–Venus fusion protein (RV-4ChopV(B19G)) or Venus^{31,32} (Fig. 2 and Extended Data Fig. 4) into NAc (250 nl) or CeM (180 nl). These virus constructs are referred to as RV-ChR2–Venus and RV-Venus in the manuscript. All animals receiving control virus injection were pooled into one control group. Injections were performed using glass micropipettes (1–5 μ l; Drummond Scientific) pulled with a puller (Narishige PC-10) mounted on 10- μ l microsyringes (Hamilton Microlitre 701; Hamilton Co.) to deliver the retrobeads at a rate of 2 nl s^{-1} or virus at a rate of 0.5 to 1 nl s^{-1} , using a microsyringe pump (UMP3; WPI) and controller (Micro4; WPI). After completion of the injection, the pipette was raised $100 \mu\text{m}$ and left for an additional 10 min to allow diffusion of the retrobeads or the virus at the injection site and then slowly withdrawn.

In a separate group of experiments (Fig. 3), adeno-associated virus serotype 5 (AAV₅) carrying halorhodopsin 3.0 fused to enhanced yellow fluorescent protein (eYFP) in a double-floxed inverted open reading frame (DIO) under the control of EF1 α promoter (AAV₅-EF1 α -DIO-eNpHR3.0-eYFP) or a corresponding fluorophore control (AAV₅-EF1 α -DIO-eYFP) was injected bilaterally into the BLA (400 nl in each hemisphere) at stereotaxic coordinates from bregma: -1.60 mm anteroposterior, ± 3.35 mm mediolateral and -4.90 mm dorsoventral. Concurrently, canine adenovirus 2 (CAV2)^{33,34} carrying Cre-recombinase (or a mixture of CAV2-Cre and herpes simplex virus carrying Cre-recombinase and the fluorescent reporter mCherry under the control of EF1 α promoter) was injected into the NAc (300 nl in each hemisphere) or CeM (150 nl in each hemisphere) at the same coordinates described above. We summarize this strategy with the designation ‘Cre-DIO’. All animals receiving fluorophore control injection were pooled into one control group. In this manuscript, CAV refers to CAV2, and NpHR refers to eNpHR3.0.

In order to deliver light to the BLA, a 300- μm diameter optic fibre (0.37 numerical aperture (NA)) glued to a 1.25 mm ferrule was implanted above the BLA (-1.64 mm anteroposterior, ± 3.35 mm mediolateral and -4.25 mm dorsoventral). One layer of adhesive cement (C&B metabond; Parkell) followed by cranioplastic cement (Dental cement; Stoelting) was used to secure the fibre ferrule to the skull and, 20 min later, the incision was sutured. Blue light ($\sim 20 \text{ mW}$, $\sim 283 \text{ mW per mm}^2$ at the fibre tip) was delivered using a 473 nm laser and yellow light ($\sim 10 \text{ mW}$, $\sim 141 \text{ mW per mm}^2$ at the fibre tip) was delivered using a 589/593 nm laser.

After surgery, body temperature was maintained using a heat lamp until the animal fully recovered from anaesthesia. Behavioural experiments followed by *ex vivo* electrophysiological recordings were conducted approximately 2 weeks after surgery. Behavioural experiments requiring expression via rabies virus were conducted 4–5 days after surgery (Fig. 2). Behavioural experiments requiring viral expression via the Cre-DIO strategy were conducted 3 months after surgery (Fig. 3).

Pavlovian conditioning. *Fear conditioning.* The mice were conditioned using behavioural hardware boxes (MedAssociate) placed in custom-made sound-attenuating chambers. Each box contained a modular test cage with an electrifiable grid floor and a speaker. On the day of conditioning, all animals were exposed to two 30 min conditioning sessions separated by 20 min in the home cage (Extended Data Fig. 1e). During the first session, mice in the unpaired group received six tone presentations, while mice in the paired group received no cues. During the second session, mice in the unpaired group received six foot shocks whereas mice in the paired group received six tones, each co-terminating with a shock (paired fear). During each session, a period of acclimation lasting 200 s preceded the presentation

of the first tone or foot shock. The conditioned stimulus consisted of a 2 kHz, 80 dB pure tone lasting 20 s. The unconditioned stimulus consisted of scrambled 1.5 mA foot shock lasting 2 s. During paired conditioning, the conditioned and unconditioned stimuli were co-terminating. Cue presentations were separated by 70 to 130 s. Following conditioning, mice were returned to their home cages for ~ 24 h until preparation of brain slices (Extended Data Fig. 1e). Videos of the mice were acquired during the second session for the paired group and both sessions for the unpaired group, to allow freezing quantification during the tone (an infrared LED was switched on during the period of the tone to synchronize CS with the video). *Measurement of fear behaviour.* Percentage time freezing during conditioned stimulus presentation (Extended Data Fig. 1f) was quantified by manual scoring with the help of custom-written software in MATLAB. For each of the six trials, a segment of the video containing 20 s of the tone and the 20 s preceding the tone was extracted frame by frame and exported into MATLAB. Two additional segments of the same duration were extracted starting at randomly chosen points in the video. The sequence of these eight trials was then randomized and presented to a human scorer who was blind to the trial number. The scores were then re-assembled and the percentage of freezing during the conditioned stimulus was calculated. Frame numbers of the video containing the tone were confirmed by generating a heat map of the intensity of the pixels containing the infrared LED. *Reward conditioning.* Twenty hours after food restriction, the mice were conditioned in sound-attenuating boxes (MedAssociates). Each box contained a modular test cage assembled with a sucrose delivery port, a speaker and a house light placed under the sucrose port. The conditioned stimulus consisted of a compound light–tone cue, ended by a beam break, 400 ms after port entry detection. If the mouse did not enter the port, the tone lasted for 30 s. The tone was a 5 kHz, 80 dB pure tone. For the paired group, a small volume (15 μl) of a sucrose solution (30%) was delivered into the port 1 s after conditioned stimulus onset, only if the mouse had entered the port after the onset of the previous conditioned stimulus, to prevent sucrose accumulation. For the unpaired group, no sucrose was delivered to the port. The inter-trial interval (ITI) of the conditioned stimulus presentations was chosen randomly from a list at runtime and was 143 ± 40 s for the first 20 conditioned stimulus presentations and 108 ± 32 s for the 100 subsequent conditioned stimulus presentations. The conditioning session was terminated after 120 sucrose deliveries and lasted for about 4 h. Performance of the mouse was assessed during the second half of a conditioning session. After the training session, the unpaired mice received the same amount of sucrose as the paired mouse (in their home cage $15 \mu\text{l} \times 120 = 1.8 \text{ ml}$, Extended Data Fig. 1e). In the paired group, if the mice did not claim all the sucrose, the remaining volume was made available to the mouse in its home cage after the conditioning session. After 20 min in their home cages, all the animals had *ad libitum* food until the electrophysiology experiment the following day.

Learning criterion for reward learning. A mouse was considered to have acquired the task (and classified as a learner) if the number of port entries from +1 s to +8 s relative to conditioned stimulus onset (Extended Data Fig. 1g, black line) was significantly higher than the number of port entries from -1 s to -8 s relative to conditioned stimulus onset (Extended Data Fig. 1g, grey line). Statistical significance was tested using a one-sided Wilcoxon rank-sum test (MATLAB) and the threshold for learning was set at $P < 0.001$.

Conditioning for photoinhibition experiments. In these experiments, the same animals experienced reward conditioning followed by fear conditioning after 1–4 weeks. Pure tones of 2 and 10 kHz were used as conditioning stimuli in these two paradigms; the use of these two tones was counterbalanced across animals. Animals were tethered using a dual commutator for light delivery. During fear conditioning, yellow light was delivered 1 s before shock onset until 1 s after shock termination (shock intensity = 0.5 mA). During reward learning, yellow light was delivered for 7.5 s immediately following a port entry during conditioned stimulus (tone) presentation.

Ex vivo electrophysiology. *Brain tissue preparation.* About 2 weeks after retrobead injections in NAc and CeM, 114 mice were anaesthetized with 90 mg kg^{-1} pentobarbital sodium and perfused transcardially with 10 ml of modified artificial cerebrospinal fluid (ACSF) at $\sim 4^\circ\text{C}$ saturated with 95% O₂ and 5% CO₂, containing: 75 mM sucrose, 87 mM NaCl, 2.5 mM KCl, 1.3 mM NaH₂PO₄, 7 mM MgCl₂, 0.5 mM CaCl₂, 25 mM NaHCO₃ and 5 mM ascorbic acid (pH 7.25–7.4, $327 \pm 3 \text{ mOsm}$). The brain was then extracted and glued (Roti coll I; Carh Roth GmbH) on the platform of a semiautomatic vibrating blade microtome (VT1200; Leica). The platform was then placed in the slicing chamber containing modified ACSF at 4°C . Coronal sections of 300 μm containing the NAc, CeM or BLA were collected in a holding chamber filled with ACSF saturated with 95% O₂ and 5% CO₂, containing: 126 mM NaCl, 2.5 mM KCl, 1.25 mM NaH₂PO₄, 1.0 mM MgCl₂, 2.4 mM CaCl₂, 26.0 mM NaHCO₃, 10 mM glucose (pH 7.25–7.4, $298 \pm 2 \text{ mOsm}$). Recordings were started 1 h after slicing and the temperature was maintained at approximately 31°C both in the holding chamber and during the recordings.

All retrobead injection sites were checked and imaged with a camera (Hamatsu) attached to the microscope (BX51; Olympus, Extended Data Fig. 1). The slice images were reported on the mouse brain atlas (Paxinos and Watson) and the centre of the injection was taken at the brightest point of the fluorescence. Some of the retrobead injections had dorsoventral leaks. In this case, the centre of the injection was taken on the brightest fluorescent point in the target structure (Extended Data Fig. 1). If the injection site was outside NAc or CeM, respective projectors of this injection were not recorded in the BLA. In addition, all the CeM injections were overlaid on the mouse atlas. CeM projector recordings collected from animals with injection sites that had leaks into CeC and/or CeL were discarded.

Whole-cell patch-clamp recording. Recordings were made from visually identified neurons containing retrobeads. Patched cells were filled with Alexa Fluor 350 and biocytin, visualized and superimposed with retrobead fluorescence to confirm whether the patched cell was retrobead positive.

For measuring AMPAR/NMDAR ratio, brain slices containing the BLA were then placed in the recording chamber perfused with ACSF containing 100 μM of the γ -aminobutyric A receptor (GABA_AR) antagonist picrotoxin (R&D systems). Picrotoxin was not used to assay passive membrane properties from NAc- and CeM-projecting BLA neurons. A bipolar stimulating electrode (~ 80 μm spacing between tips) was placed in the amygdala–striatal transition zone containing internal capsule fibres (Extended Data Fig. 2). Electric stimulation intensity was between 0.01 and 0.2 mA. For electrophysiological characterization of NAc and CeM projectors (Fig. 3a–g) and confirmation of the health of rabies-virus-transduced cells (Extended Data Fig. 7), picrotoxin was not added to the ACSF.

Voltage-clamp recordings were made using glass microelectrodes (4–6 M Ω) shaped with a horizontal puller (P-1000) and filled with a solution containing: 120 mM caesium methansulphonate, 20 mM HEPES, 0.4 mM EGTA, 2.8 mM NaCl, 5 mM tetraethylammonium chloride, 2.5 mM MgATP, 0.25 mM NaGTP, 8 mM biocytin and 2 mM Alexa Fluor 350 (pH 7.3, 283 mOsm). The cells were first clamped at -70 mV to determine optimal intensity for the electric stimulation of the internal capsule. Current-clamp recordings to characterize electrophysiological properties of NAc and CeM projectors were made using similar glass microelectrodes (4–6 M Ω) filled with a solution containing: 125 mM potassium gluconate, 20 mM HEPES, 10 mM NaCl, 3 mM MgATP, 8 mM biocytin and 2 mM Alexa Fluor 350 (pH 7.3; 283 mOsm).

Recorded signals were amplified using Multiclamp 700B amplifier (Molecular Devices). Analogue signals were digitized at 10 kHz using a Digidata 1440 and pClamp9 software (Molecular Devices). ACSF and drugs were applied to the slice via a peristaltic pump (Minipuls3; Gilson) at 3 ml per min.

All recordings were performed blind to the performance of the animal, and a subset of the data was obtained blind to the behavioural conditioning group of the animal. We recorded the position of the cells within the BLA (Extended Data Fig. 2) and the placement of the stimulating electrode relative to the BLA. There was no observable difference in either of these parameters across slices obtained from animals in different behavioural conditioning groups.

In order to obtain the AMPAR/NMDAR ratio, the cell was first voltage clamped at $+40$ mV. Once we obtained a stable baseline excitatory post-synaptic current (EPSC) amplitude in response to internal capsule fibre stimulation (compound AMPAR + NMDAR current), we bath applied the NMDAR antagonist AP5 (D-(-)-2-amino-5-phosphonopentanoate; R&D systems) at a concentration of 50 μM . AMPAR EPSCs were recorded starting from 5 min after the action of AP5. NMDAR current was obtained by subtracting the average EPSC trace of the AMPAR current from the compound current. Each group in Fig. 1 included 9–13 neurons recorded from 6–9 mice.

Histology. The location of all recorded neurons was checked after the recording. Co-localization of Alexa Fluor 350 and retrobeads was confirmed at the end of the recording, and double-checked with confocal microscopy for the cells that were recovered with streptavidin staining. For each experiment, the slices containing a retrobead injection site (NAc and CeM) or a recorded neuron (BLA) were fixed overnight at 4 °C in 4% paraformaldehyde (PFA), and then kept in phosphate buffered saline (PBS). Slices containing patched neurons were incubated for 2 h in streptavidin-CF405 (2 mg ml⁻¹, dilution 1:500; Biotium), mounted on microscope slides with PVA-DABCO and imaged under the confocal microscope (Extended Data Fig. 3).

Data analysis. Offline analysis of AMPAR/NMDAR ratios, paired-pulse ratios and electric properties was performed using Clampfit (Molecular Devices) and MATLAB software written by P.N. Membrane properties including access resistance of the cell were computed by a MATLAB implementation of the Q-method³⁵. All custom-written software is available upon request.

In vivo optogenetic behaviour. **Light delivery.** For optical stimulation during behavioural assays (Fig. 2), a 473 nm (blue light) or 589/593 nm laser (yellow light) (OEM Laser Systems) was connected to a patch cord with a pair of FC/PC

connectors in each end (Doric). This patch cord was connected through a fibre optic rotary joint (which allows free rotation of the fibre; Doric) with another patch cord with an FC/PC connector on one side and a ferrule connection on the other side (matching the size of the ferrule glued to the optic fibre implanted in the mouse). The optic fibre implanted in the mouse (300 μm diameter, 0.37 NA) was connected to the optic patch cord using ceramic mating sleeves (PFP). Blue light was delivered at 20 mW in 20 Hz, 5 ms light pulses. Yellow light was delivered at 10 mW, for 4 s during fear conditioning and 7.5 s during reward conditioning. Laser output was modulated with a Master 8 pulse stimulator (A.M.P.I.). Onset of laser pulses was determined by behavioural hardware (MedPC Associates).

Intracranial optical self-stimulation (ICSS). 4.5 days after surgery, mice were food-restricted overnight. Immediately before the start of each session, fibre optic implants were connected to a patch cord and the mouse was placed in conditioning chambers equipped with active and inactive nose-poke ports directly below two cue lights, as well as auditory stimulus generators and video cameras. Mice were given two self-stimulation sessions on two consecutive days (5.5 and 6.5 days after surgery) in which they could respond freely at either nose-poke port. On day 1 both nose-poke ports were baited with a crushed cereal treat to facilitate initial investigation. The start of each 2 h session was indicated by the illumination of both nose-poke ports and the onset of low-volume white noise to mask unrelated sounds. Each nose poke in the active port resulted in light stimulation of BLA projectors (60 pulses, 20 Hz, 5 ms pulse duration). Concurrently, the cue-light above the respective port was illuminated and a distinct 1-s tone was played for each nose poke (1 kHz and 1.5 kHz counterbalanced), providing a visual and auditory cue whenever a nose poke occurred. Active and inactive nose-poke time stamps were recorded using Med-PC software and day 2 data were analysed using MATLAB and Microsoft Excel.

Real-time place avoidance (RTPA). The RTPA chamber was constructed from transparent plastic (50 \times 53 cm) and divided into two equal compartments. One of these was assigned as the photo-stimulated zone (counterbalanced between animals). At the start of the 1 h session, individual mice were placed in the non-stimulated side of the chamber. Every time the mouse crossed to the side of the chamber paired with photostimulation, 20 Hz (~ 20 mW, 5 ms pulse duration) laser stimulation was delivered until the mouse crossed back into the non-stimulated side. Ethovision XT video tracking software (Noldus Information Technologies) was used to track the animal and control the onset and offset of light pulse trains. Data were subsequently analysed using MATLAB and Microsoft Excel software.

Histology. After optogenetic experiments, all mice were anaesthetized with pentobarbital sodium, and transcardially perfused with ice-cold Ringer's solution followed by ice-cold 4% PFA in PBS (pH 7.3). Extracted brains were fixed in 4% PFA overnight and then equilibrated in 30% sucrose in PBS. 40- μm thick coronal sections were sliced using a sliding microtome (HM430; Thermo Fisher Scientific) and stored in PBS at 4 °C until they were processed for histology. Sections were then incubated with a DNA-specific fluorescent probe (DAPI: 4',6-diamidino-2-phenylindole (1:50,000)) for 30 min, and finally washed with 1 \times PBS followed by mounting on microscope slides with PVA-DABCO.

Imaging. Confocal fluorescence images were acquired on an Olympus FV1000 confocal laser scanning microscope using a 10 \times /0.40 NA objective for viral injections and fibre placements imaging or a 40 \times /1.30 NA or 60 \times /1.42 NA oil-immersion objectives for imaging streptavidin-CF405 stained neurons. The centre of the viral injection was taken at the brightest fluorescent point in anteroposterior, mediolateral and dorsoventral axis. The tip of the fibre was determined by the ~ 50 - μm thick gliosis generated by the fibre. Neurons recovered from the streptavidin staining ($\sim 60\%$ recorded in the whole cell) were imaged covering the whole dendritic and axonal arborization contained in the slice.

Neuron reconstructions. Imaris software (Bitplane Inc.) was used to reconstruct neurons from z-stacks of confocal images and to perform Sholl analysis³⁶. Since we are reconstructing neurons filled during whole-cell patch clamp recordings, we chose to focus solely on dendritic branching patterns and did not examine parameters such as the volume of the soma, since this measure might be compromised by experimental procedures. Overlaying the atlas on images of brain slices revealed that the distances depicted in the atlas are about 90% smaller than physical distances in brain slices. For example, if the length of a brain region is 900 μm in the atlas, then the real distance measured in our brain sections was about 1000 μm . Therefore, to depict the reconstructed neurons (Fig. 4h, i and Extended Data Fig. 8), we multiplied physical distances by a factor of 0.9.

RNA sequencing (RNA-seq). **Manual cell sorting and RNA sequencing.** The RNA-seq experiment was repeated twice to verify reproducibility, and we refer to these biological replicates as experiment 1 and experiment 2 (see Extended Data Fig. 9c: samples used in experiment 1 and 2 are indicated in black ($n = 9$) and blue ($n = 8$) respectively below the heatmap). Manual sorting of fluorescent cells were carried out as described in ref. 37. In brief, adult C57Bl6 male

mice (~6–8-weeks-old at surgery, C57BL/6NcrJ for experiment 1, C57BL/6J for experiment 2) were injected with red fluorescent retrograde beads into either NAc or CeM. Surgeries for experiment 1 were conducted at Harvard Medical School by P.N. and surgeries for experiment 2 were conducted at MIT by G.G.C. About 2 weeks after surgery, animals were decapitated under isoflurane anaesthesia and their brain was quickly removed and transferred into ice-cold oxygenated ACSF, containing 126 mM NaCl, 20 mM NaHCO₃, 20 mM dextrose, 3 mM KCl, 1.25 mM NaH₂PO₄, 2 mM CaCl₂, 2 mM MgCl₂, 50 μM AP5, 20 μM DNQX and 100 nM TTX. Acute 330-μm coronal brain slices were prepared and incubated in a protease (1.2 mg ml⁻¹ protease E; Sigma-Aldrich) containing oxygenated ACSF for 50 min. After 15 min of washes in the ACSF, BLA tissue was microdissected using a pair of fine scissors under a fluorescent dissecting microscope (Leica M165FC stereomicroscope). The dissected BLA tissue was then triturated in ACSF using a series of three Pasteur pipettes of decreasing tip diameters and the dissociated cells were transferred into a small Petri dish. With visual control under a fluorescent dissecting microscope, red-retrograde-positive neurons were aspirated into a micropipette with a 30–50 μm tip diameter and transferred into a clean Petri dish. A total of 35–60 retrograde-positive neurons were pooled for each sample, which were immediately lysed in 50 μl of extraction buffer (PicoPure RNA isolation kit, Arcturus, Life Technologies) and total mRNA was subsequently isolated. Complementary DNA was synthesized using Ovation RNA-seq System V2 kit (Neugen). We obtained approximately 6 μg of cDNA from 35–60 cells from each group. Then, the cDNA library was prepared using Ovation Ultralow DR Multiplex Systems (Nugen). Sequencing was conducted on an Illumina HiSeq2500 using single-end 50 base pairs at the Biopolymer facility, Harvard Medical School (for experiment 1), and an Illumina NextSeq 500 using single-end 75 base pairs with high flow cell size at the FAS centre for systems biology, Harvard University (for experiment 2). The total number of reads that we obtained for each sample were approximately 34 million (for experiment 1) and 50 million (for experiment 2).

Analysis of RNA-seq data. Sequencing reads were mapped using Tophat version 2.0.10 (<http://ccb.jhu.edu/software/tophat/index.shtml>) against the *Mus musculus* UCSC version mm10 genome. After alignment, the read counts for each gene were extracted using HTseq (<http://www-huber.embl.de/users/anders/HTSeq/doc/overview.html>) based on the mm10 Refseq gff file. Log₂ fold differences were computed from each of two independent experiments using DESeq2. Candidate differentially expressed genes were required to be enriched in CeM or NAc projectors at a quantile fold-difference threshold of 0.01 (Fig. 4) or 0.02 (Extended Data Fig. 9) in each of two independent experiments ($n = 8$, NAc; $n = 9$, CeM total). To estimate false discovery rate (Extended Data Fig. 9), we used two types of chance estimates. One of the chance estimates, 'flip-flopped', is taken from genes that passed the quantile thresholds but were enriched in opposite populations in the two experiments. Another chance estimate, 'permuted', is determined based on permuting fold differences across genes within each independent experiment (Extended Data Fig. 9). We estimated false discovery rate using the more conservative chance estimate, flip-flopped with the following formula: (number of genes on the flip-flopped list/number of genes on the differentially expressed genes). RNA-seq data has been deposited in the Gene Expression Omnibus under accession code GSE66345

Statistical analysis. Statistical analyses were performed using commercial software (GraphPad Prism; GraphPad Software, Inc.). Within-subject comparisons were made using paired tests. Group differences were detected using either one-way analysis of variance (ANOVA) or with two-way ANOVA, both followed by Bonferroni post-hoc tests. Corrections for multiple comparisons were made when appropriate. The reported numbers of degrees of freedom (df) for each one-way ANOVA are between column degrees of freedom and total degrees of freedom. Since normality tests have little power to detect non-gaussian distributions with small data sets, we did not explicitly test for the normality of our data sets. We used the Grubbs' test to detect and remove outliers from our data. Single-variable differences were detected with two-tailed paired or unpaired (as noted) Student's *t*-tests. For all results, the significance threshold was placed at $\alpha = 0.05$ ($*P < 0.05$, $**P < 0.01$, $***P < 0.001$), and corrections for multiple comparisons were reflected in the *P* value rather than in α . All data are shown as mean and s.e.m. To assess learning during the reward task, we used a one-sided Wilcoxon rank-sum test (MATLAB) and set the threshold for learning at $P < 0.001$. Result sheets of statistical tests from GraphPad software detailing (wherever applicable) estimates of variance within each group, confidence intervals, effectiveness of pairing (in case of paired *t*-tests), comparison of variances across groups, etc. are available upon request.

Sample size. The target number of samples in each group was determined based on numbers reported in published studies. No statistical methods were used to predetermine sample size. In the photoinhibition experiment, since the viral incubation time was long, we factored in the skill of the surgeon to determine

the number of surgeries to be performed. Our target number of animals in each group was 12. The experimenter performing surgeries was known to hit the targets used (NAc, CeM, BLA) with a probability of 0.9. Since there were six targets in each brain (three in each hemisphere—two injections and one optical fibre), the probability of a successful surgery would be approximately $(0.9)^6 \approx 0.5$. We therefore performed about 24 surgeries in each group. All sample sizes mentioned in figures represent biological replicates. All animals receiving control virus injections were pooled into one control group (Figs 2 and 3). In the Venus group from Fig. 2c, there were six animals with injections in NAc and six animals with injections in CeM. In the Venus group from Fig. 2e, there were four animals with injection in NAc and two animals with injection in CeM. In the eYFP group from Fig. 3b, there were ten animals with injections in NAc and six animals with injections in CeM. In the eYFP group from Fig. 3c, there were nine animals with injections in NAc and five animals with injections in CeM.

Replication. Results from AMPAR/NMDAR ratio experiments were replicated once with a different experimenter and the final numbers reported in the paper are pooled across both repetitions of the experiment (Fig. 1). Photostimulation and photoinhibition experiments (Figs 2 and 3) were not replicated. The RNA-seq experiment was also replicated once (Fig. 4).

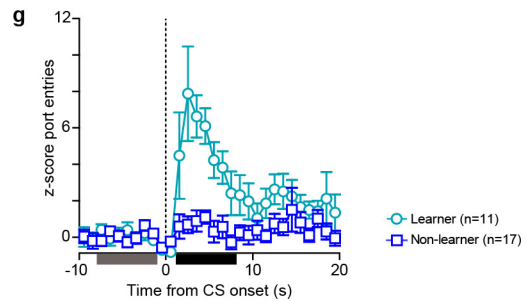
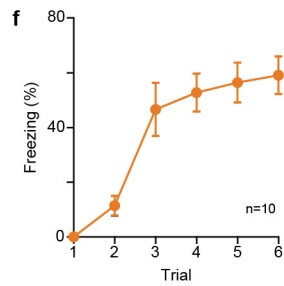
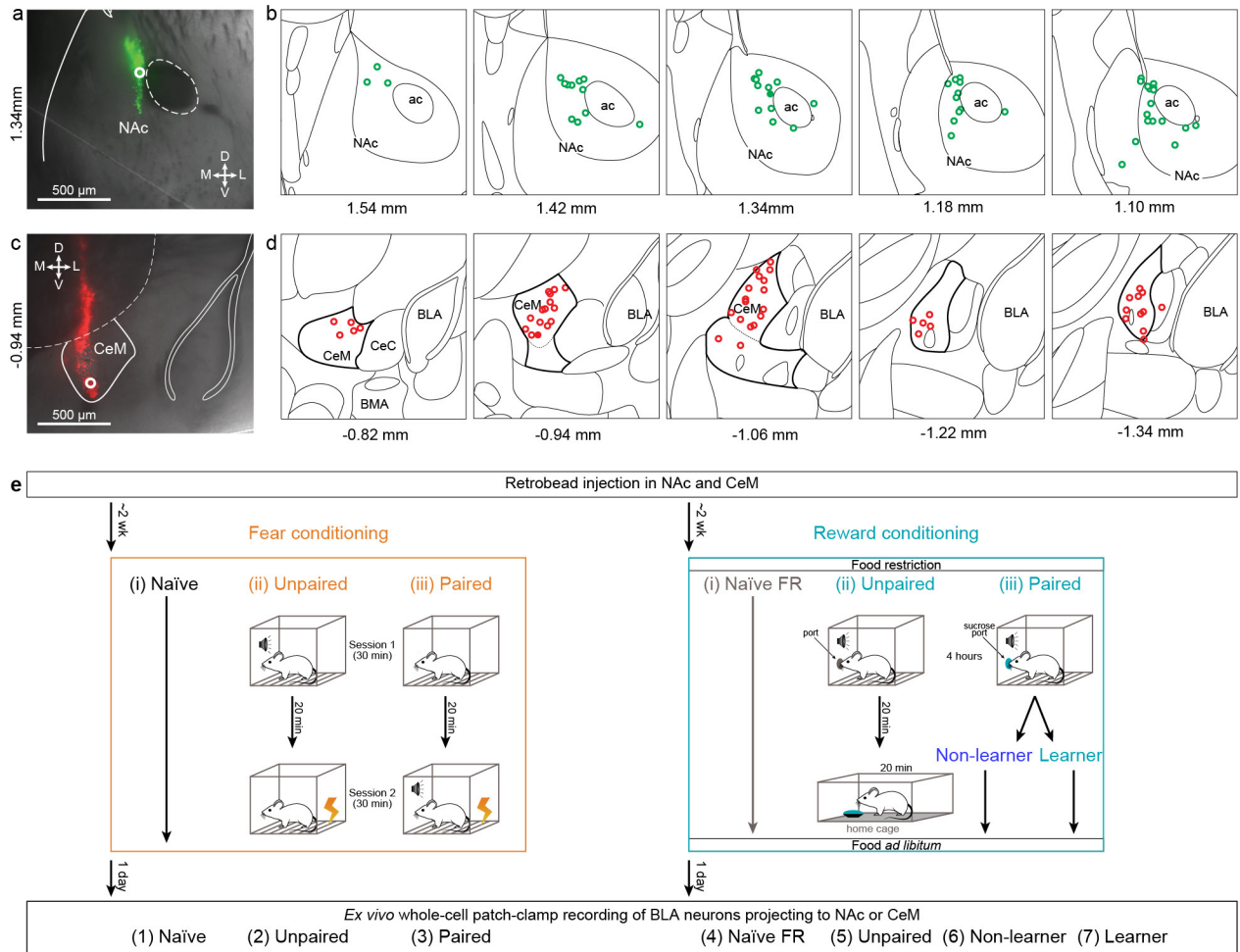
Randomization. All surgical and behavioural manipulations performed on each animal were determined randomly. All randomization was performed by an experimenter, and no explicit randomization algorithm was used. For animals used in photostimulation and photoinhibition experiments, the virus used in each animal (Chr2/Venus or NpHR/eYFP) and injection site (NAc/CeM) were determined randomly and the stereotaxic apparatus used for surgery was counterbalanced across groups. For surgeries with unilateral injections and/or fibre placements, the hemisphere used for injections was determined randomly during the time of the surgery. Surgeries were performed on animals caged in groups of 4 or 5 animals. Animals from each cage were allocated to at least two behavioural groups. All animals used in *ex vivo* electrophysiology experiments were isolated at least 1 day before behavioural conditioning.

Exclusion criteria. *Ex-vivo electrophysiology.* Data were excluded based on pre-determined histological and electrophysiological criteria, established during pilot experiments. The injection site was determined as the most ventral point where fluorescence was brightest, and data from cells where the corresponding retrograde injection was outside the target region (NAc or CeM) were excluded (Extended Data Fig. 1a–d). Each recorded cell was confirmed to be a projector by overlaying the fluorescence from retrobeads with the fluorescence from Alexa Fluor dye contained in the pipette. Each cell was also confirmed to be in the BLA by visualizing with differential interference contrast microscopy under a 4× objective. We did a secondary confirmation under the confocal microscope for cells that were recovered from streptavidin staining. Cells in which evoked responses were polysynaptic (multiple peaks in the evoked current) were discarded. Data from cells whose access resistance was greater than 40 MΩ or cells that died during recording were also excluded.

Animals used in photostimulation and photoinhibition experiments. Data from animals used in photostimulation and photoinhibition experiments (Figs 2 and 3) were excluded based on histological and performance criteria established during pilot experiments. Histological criteria included injection sites and optical fibre placement (Extended Data Figs 4 and 5). Only animals with injection sites in the region of interest (NAc or CeM) were included. For animals with a rabies virus injection in CeM, atlas outlines were overlaid manually over a confocal image of the BLA containing the damage caused by the tip of the optic fibre. Light cones based on numerical aperture of the optic fibre (NA 0.37, ~15° half angle) were then drawn below the optic fibre and animals in which light cones encompassed central amygdala were excluded from further analysis. For the optical self-stimulation experiment, data from animals that did not respond at least 40 times (sum of nose pokes in active and inactive ports) over the 2 hour period were excluded from further analysis. For photoinhibition experiments, the amount of expression in each hemisphere of the BLA was rated on a scale of 0–5 based on fluorescence intensity by an experimenter blind to the behavioural performance of the animal. These ratings were gathered in an excel sheet, read by a MATLAB script and only data from animals with fluorescence ratings greater than 4 in each hemisphere were included for further analysis.

31. Kiritani, T., Wickersham, I. R., Seung, H. S. & Shepherd, G. M. G. Hierarchical connectivity and connection-specific dynamics in the corticospinal–corticostriatal microcircuit in mouse motor cortex. *J. Neurosci.* **32**, 4992–5001 (2012).
32. Wickersham, I. R., Sullivan, H. A. & Seung, H. S. Production of glycoprotein-deleted rabies viruses for monosynaptic tracing and high-level gene expression in neurons. *Nature Protocols* **5**, 595–606 (2010).
33. Soudais, C., Boutin, S. & Kremer, E. J. Characterization of cis-Acting Sequences Involved in Canine Adenovirus Packaging. *Mol. Ther.* **3**, 631–640 (2001).

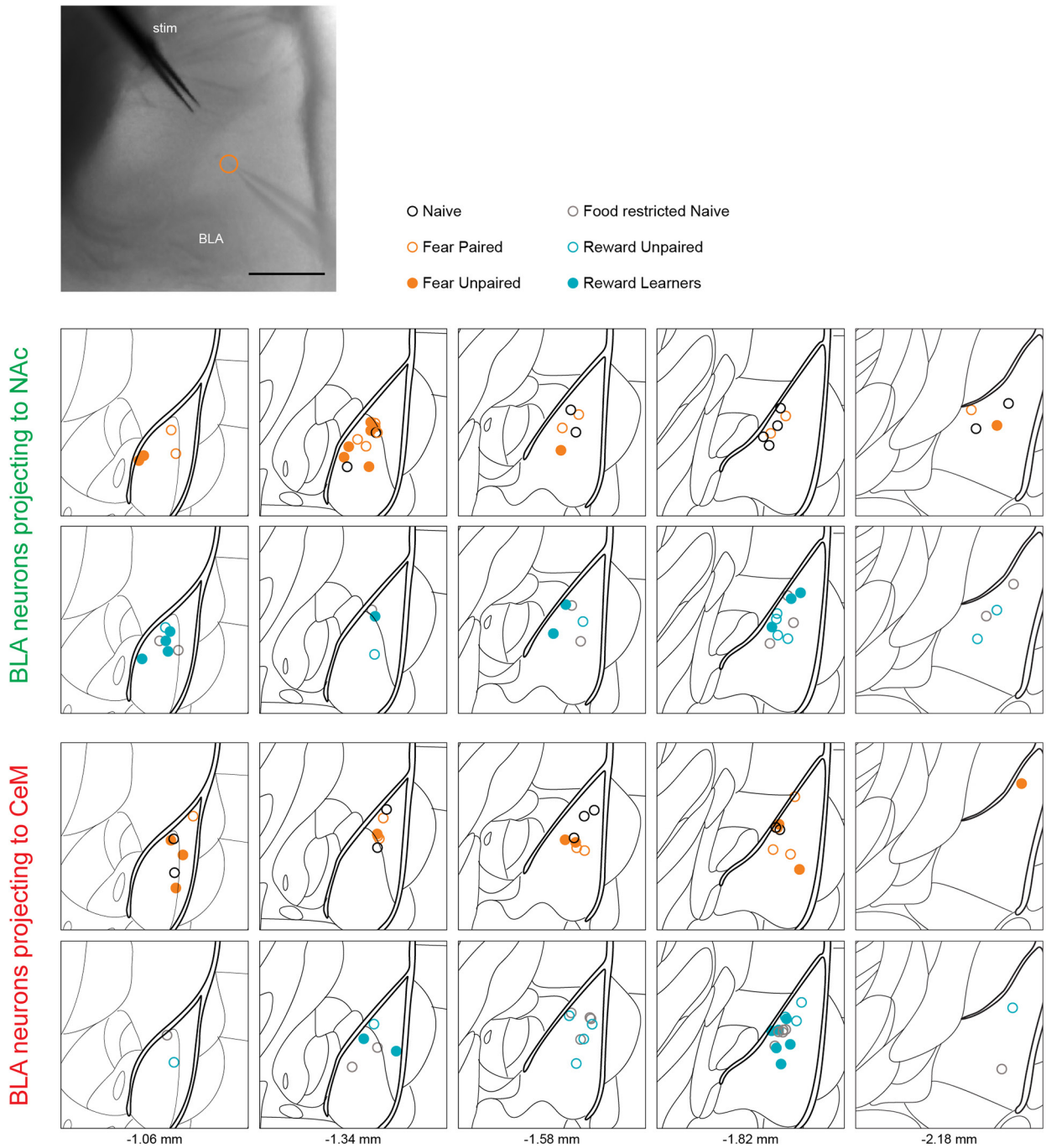
34. Hnasko, T. S. *et al.* Cre recombinase-mediated restoration of nigrostriatal dopamine in dopamine-deficient mice reverses hypophagia and bradykinesia. *Proc. Natl Acad. Sci. USA* **103**, 8858–8863 (2006).
35. Novák, P. & Zahradník, I. Q-method for high-resolution, whole-cell patch-clamp impedance measurements using square wave stimulation. *Ann. Biomed. Eng.* **34**, 1201–1212 (2006).
36. Sholl, D. A. Dendritic organization in the neurons of the visual and motor cortices of the cat. *J. Anat.* **87**, 387–406 (1953).
37. Hempel, C. M., Sugino, K. & Nelson, S. B. A manual method for the purification of fluorescently labeled neurons from the mammalian brain. *Nature Protocols* **2**, 2924–2929 (2007).



Extended Data Figure 1 | Histological verification of retrobead injection sites and behavioural quantification of fear and reward conditioning for mice used in Fig. 1.

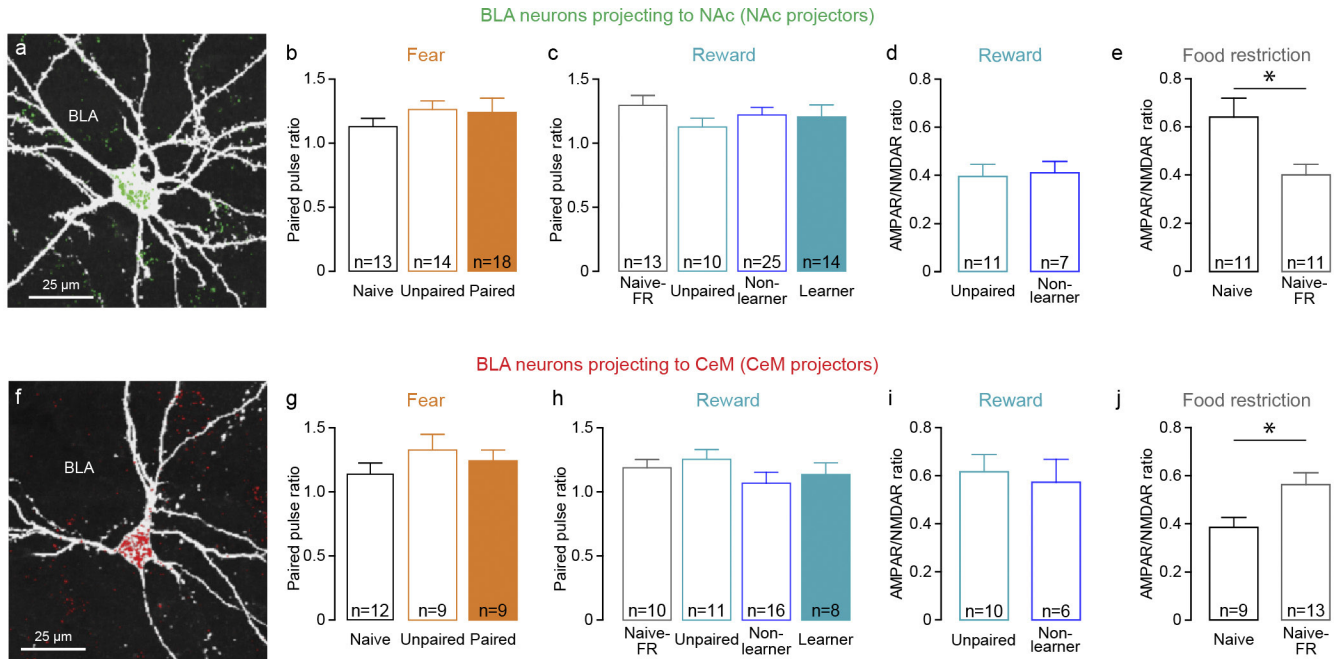
a, Representative differential interference contrast (DIC) image of a 300- μm thick coronal slice containing the centre of the retrobead injection in NAc. The white circle indicates the most ventral point at which fluorescence is brightest and corresponds to the filled green circle in **b**. **b**, Location of all retrobead injection sites (green circles) in the NAc for all mice used in Fig. 1. Each atlas schematic represents a 1.5 mm \times 1.5 mm region of the atlas and the corresponding anteroposterior stereotaxic coordinate relative to Bregma is indicated below. **c**, Representative DIC image of a 300- μm thick coronal slice containing the centre of the retrobead injection in CeM as indicated by the white dot. **d**, Retrobead injection sites in CeM (red circles) for all mice used in Fig. 1, with the example from **c** indicated by the filled red circle. The corresponding anteroposterior stereotaxic coordinate relative to Bregma is indicated below. **e**, Experimental design for AMPAR/NMDAR ratios from Fig. 1. Either red or green retrobeads were injected in the NAc and the other colour in the contralateral CeM. Two weeks after injection, the retrobeads had travelled back to the cell bodies of the BLA neurons projecting to NAc or CeM. Animals were conditioned 1 day before *ex vivo* whole-cell patch-clamp recordings. Each mouse received one of six conditioning protocols, three protocols categorized under 'fear conditioning' and three protocols categorized under 'reward conditioning'. Fear conditioning protocols: (i) naive, animals were naive to the operant chamber. (ii) Unpaired, animals were exposed to the conditioning chamber in two sessions. Animals received six tones in the first session and they received six foot shocks in the second session. Animals were returned to their home cage for \sim 20 min between the two sessions. (iii) Paired, animals were exposed to the operant chamber in two sessions. Animals did not receive any tone or shock stimuli in the first session, and received tones co-terminating with shocks in the second session. Animals were returned to their home cage for 20 min between the two sessions. Protocols for unpaired and paired fear groups were adapted from ref. 18. Reward conditioning protocols: (i) naive food restricted (FR), animals naive to the operant chamber were food restricted two days before *ex vivo* experiments and had free access to food for 1 day before *ex vivo* experiments. We used this group to control for changes in synaptic strength caused by food restriction which was necessary in reward conditioning groups to expedite task acquisition, adapted from rats as in refs 1 and 2. (ii) Unpaired, animals received tones in the operant chamber, were

returned to their home cage for \sim 20 min after which they had free access to 1.8 ml of sucrose, followed by free access to food until *ex vivo* experiments. (iii) Paired, sucrose was delivered into a port 1 s after the onset of a tone, and the tone was terminated 400 ms after the animal entered the port to claim sucrose. The tone lasted for a maximum length of 30 s. If there was sucrose in the port during the onset of a tone (indicated by the absence of a port entry after the previous tone), then no sucrose was delivered in that trial. Mice could receive up to 120 sucrose deliveries and the conditioning session lasted about 4 h after which they had free access to food until *ex vivo* experiments. Behavioural performance from the second half of the conditioning session was used to assess performance and mice that met learning criterion (see Methods) were categorized in the learner group and the rest of the mice were categorized in the non-learner group. One day after conditioning, BLA neurons identified as either NAc or CeM projectors (retrobead positive) were recorded with whole-cell patch-clamp in *ex vivo* brain slices. *Ex vivo* data from both NAc and CeM projectors were collected from the following 7 groups: (1) naive ($n = 12$ mice, 9 for NAc pr., 7 for CeM pr.); (2) unpaired fear ($n = 13$ mice, 7 for NAc pr., 9 for CeM pr.); (3) paired fear ($n = 10$ mice, 7 for NAc pr., 7 for CeM pr.); (4) naive food restricted ($n = 11$ mice, 7 for NAc pr., 8 for CeM pr.); (5) unpaired ($n = 11$ mice, 7 for NAc pr., 5 for CeM pr.); (6) reward paired non-learner ($n = 9$ mice, 5 for NAc pr., 6 for CeM pr.); and (7) reward paired learner ($n = 10$ mice, 8 for NAc pr., 7 for CeM pr.) groups. The n values indicated here are the number of mice used in Fig. 1. Data from groups 1–5 and 7 are shown in Fig. 1 and Extended Data Figs 1, 2 and 3. Data from group 6 is shown only in Extended Data Fig. 3. **f**, Time course of percentage freezing for the paired fear group. Percentage freezing was estimated during the shock-predictive tone (excluding the final 2 s, where the foot shock was delivered). **g**, Average normalized histogram of port entries relative to the onset of the tone predicting sucrose delivery for mice that learned the conditioned–unconditioned stimulus association (learners, $n = 11$) and mice that did not (non-learners, $n = 17$; see Extended Data Fig. 3). Mice in the paired reward conditioning group were deemed learners if the number of port entries in the post-conditioned-stimulus period (1 to 8 s relative to conditioned stimulus onset, black line) were determined as significantly higher than the number of port entries in the pre-conditioned stimulus period (-8 to -1 s relative to conditioned stimulus onset, grey line) using a one-sided Wilcoxon rank sum test ($P < 0.001$).



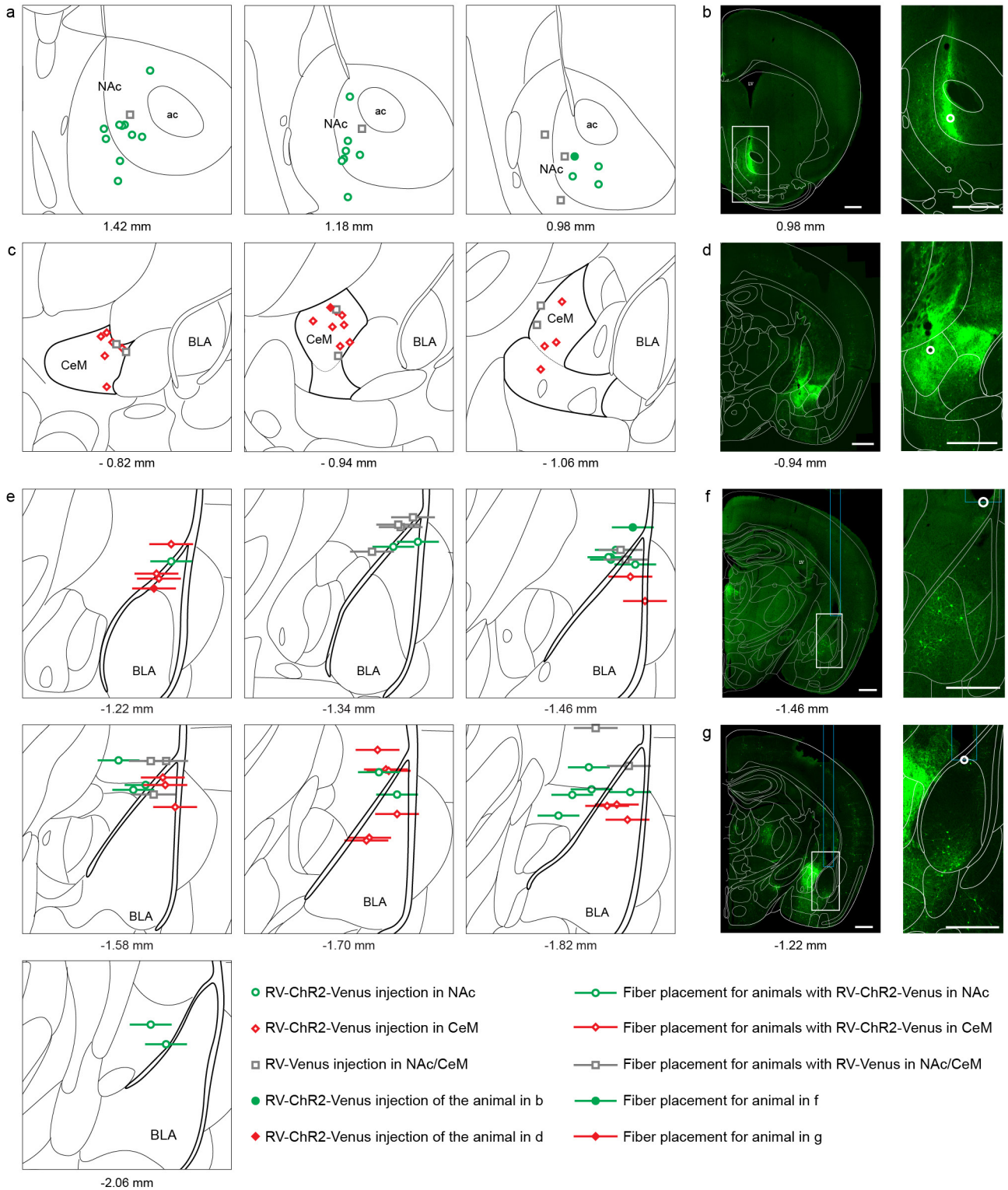
Extended Data Figure 2 | Location of BLA projectors recorded and analysed for each experimental group in Fig. 1. Top, representative DIC image showing the location of the stimulation electrode around a bundle of fibres of the internal capsule and a neuron recorded in the BLA (at the tip of the micropipette). The location of the recorded cell is indicated by an orange open circle. Scale bar, 200 μ m. Bottom, atlas schematics (1.5 mm \times 1.5 mm) showing

BLA at various anteroposterior positions relative to Bregma. Each circle represents the location of a neuron from which the AMPAR/NMDAR ratio was acquired (Fig. 1). NAc projector locations are summarized in rows 1 and 2 and CeM projector locations are summarized in rows 3 and 4. Colour of the circle represents the conditioning group of the animal from which the AMPAR/NMDAR ratio was acquired.



Extended Data Figure 3 | Paired-pulse ratio and AMPAR/NMDAR ratio in non-learners and food-restricted naive animals. **a**, Confocal image of a representative retrobead-positive neuron recorded in BLA after injection of retrobeads into NAc. This cell was recorded in an *ex vivo* slice, filled with biocytin and stained with streptavidin-CF405, pseudo-coloured white. **b**, In NAc projectors, the ratio of EPSC amplitude in response to paired-pulse stimulation (50 ms inter-pulse interval) of internal capsule inputs to the BLA was not related to experimental conditions of fear (one-way ANOVA, $F_{2,44} = 0.5209$, $P = 0.5978$). **c**, Paired-pulse ratio of EPSC amplitude was not related to experimental conditions of reward (one-way ANOVA, $F_{3,61} = 0.5868$, $P = 0.6261$). **d**, AMPAR/NMDAR ratio of internal capsule inputs onto NAc projectors in mice with unpaired tone and sucrose presentations (unpaired) and mice that did not learn the cue-reward association (non-learner) were not different (unpaired t -test $t_{16} = 0.180$, $P = 0.8595$). Both groups of mice received

the same amount of total sucrose. **e**, AMPAR/NMDAR ratio on NAc projectors is significantly decreased by food restriction in naive mice (unpaired t -test, $t_{20} = 2.626$, $P = 0.0162$). **f**, Confocal image of a representative retrobead-positive neuron recorded in BLA after retrobead injection in CeM. **g**, Paired-pulse ratio of EPSC amplitude onto CeM projectors is not related to experimental conditions of fear (one-way ANOVA, $F_{2,29} = 0.9040$, $P = 0.4169$). **h**, Paired-pulse ratio of EPSC amplitude is not related to experimental conditions of reward (one-way ANOVA, $F_{3,44} = 0.9770$, $P = 0.4129$). **i**, AMPAR/NMDAR ratio on CeM projectors is similar in unpaired reward and paired reward non-learner mice (unpaired t -test $t_{14} = 0.381$, $P = 0.7090$). **j**, AMPAR/NMDAR ratio of internal capsule inputs onto CeM projectors is significantly increased by food restriction in naive mice (unpaired t -test $t_{20} = 2.526$, $P = 0.0201$). Results show mean and s.e.m.



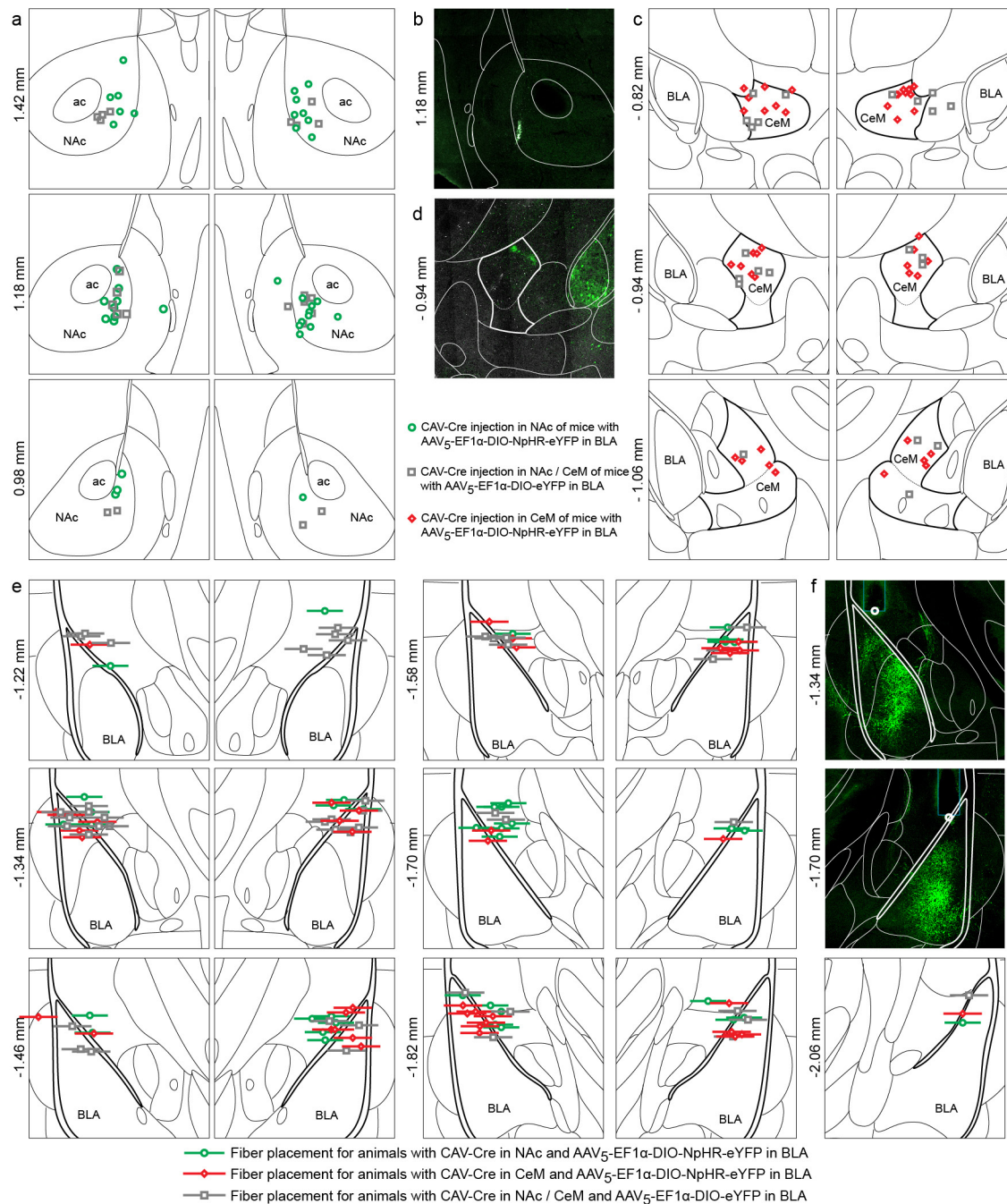
Extended Data Figure 4 | Histological verification of viral injection site and fibre placement for photostimulation experiments used in Fig. 2.

a, Center of the rabies virus injection in NAc for the animals tested in intra-cranial self-stimulation (ICSS) and real-time place avoidance (RTPA) paradigms (Fig. 2a–e). Rabies virus (RV)-ChR2-Venus injections are denoted with green circles, and RV-Venus injections are indicated with grey squares.

b, Representative confocal image of viral expression in a mouse 6 days after RV-ChR2-Venus injection in NAc. Right panel, enlarged view of the brightest fluorescence point (white circle), corresponding to the filled green circle in **a**.

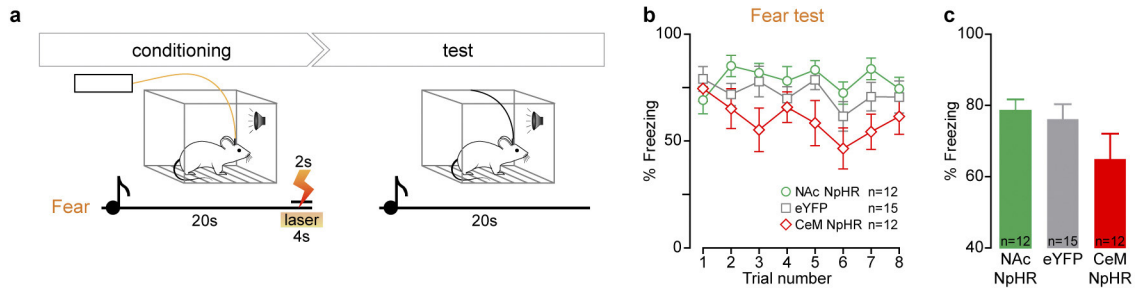
c, Center of RV-ChR2-Venus (red diamonds) and RV-Venus (grey squares) injections in CeM of animals analysed in Fig. 2. **d**, Example of viral expression 6 days after RV-ChR2-Venus injection in CeM. Right panel, enlarged view of the brightest fluorescence point (white circle), corresponding to the filled red

diamond in **c**. **e**, Optical fibre tip placements over BLA of animals with RV-ChR2-Venus injected in NAc (green circles), CeM (red diamonds) or RV-Venus in NAc or CeM (grey squares). Horizontal lines represent the thickness of the implanted fibre (300 μm). **f**, Representative confocal image showing optical fibre tip from a RV-ChR2-Venus injection in NAc, corresponding to the filled green circle in **e**. Region in the white rectangle is magnified in the right panel and shows rabies-virus-expressing NAc projectors. **g**, Representative optic fibre placement for RV-ChR2-Venus injection in CeM, corresponding to the filled diamond in **e**. Right panel: enlarged image of the BLA, containing rabies-virus-expressing CeM projectors. Atlas schematic in **a**, **c** and **e** represent 1.5 mm \times 1.5 mm of the brain and the corresponding anteroposterior coordinates relative to Bregma are specified below. Scale bars in **b**, **d**, **f** and **g** are 500 μm .



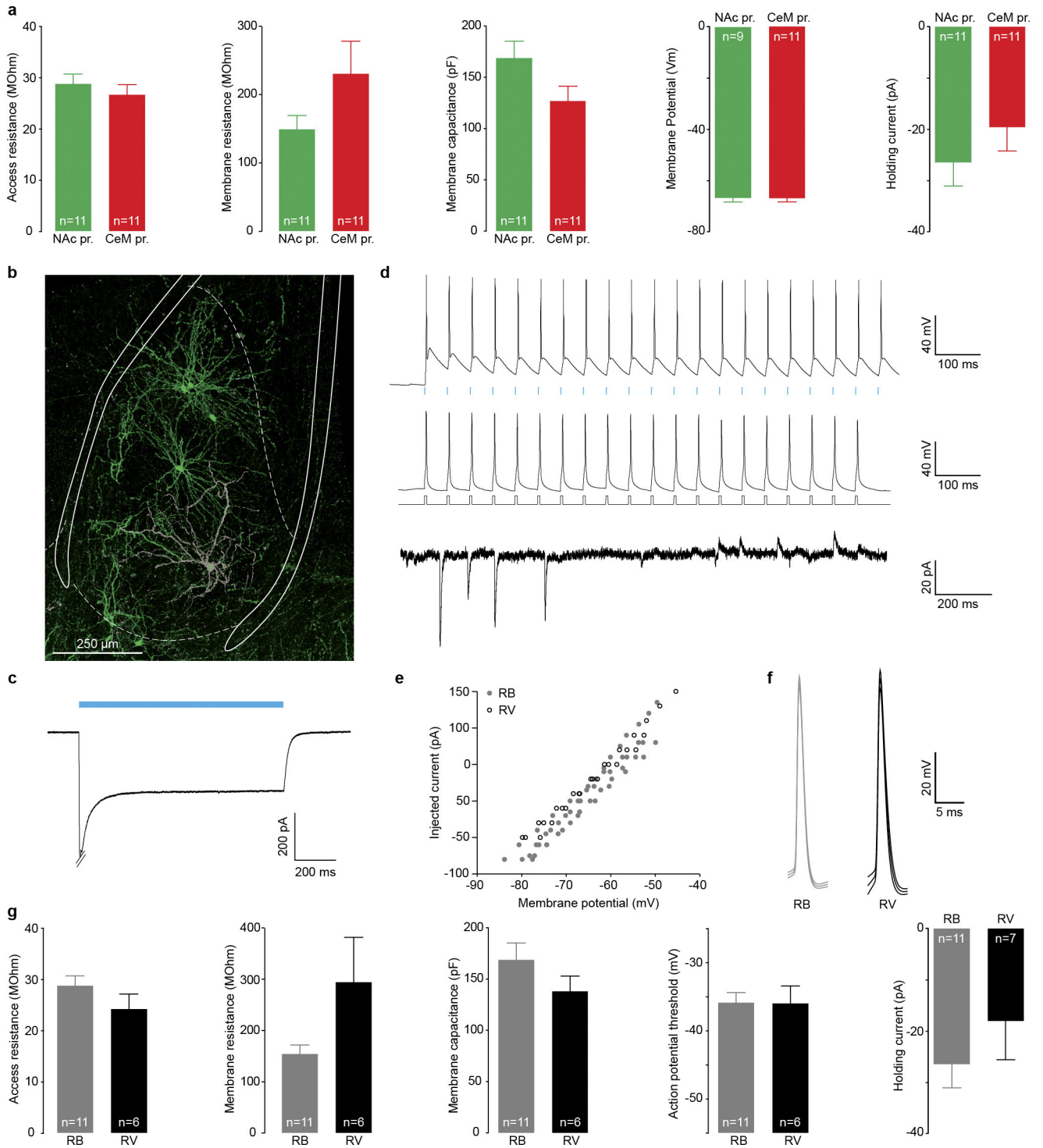
Extended Data Figure 5 | Histological verification of viral injection site and fibre placement for photoinhibition experiments used in Fig. 3. a, Centre of canine adenovirus (CAV)-Cre injection into bilateral NAc of mice with AAV₅-EF1 α -DIO-NpHR-eYFP (green circles) or AAV₅-EF1 α -DIO-eYFP (grey squares) injected bilaterally into the BLA. This approach allows for selective expression of NpHR-eYFP/eYFP, in NAc-projecting BLA neurons. **b**, Representative confocal image of the CAV-Cre injection site in NAc. **c**, Center of CAV-Cre injection into CeM from both hemispheres of mice with AAV₅-EF1 α -DIO-NpHR-eYFP (red diamonds) or AAV₅-EF1 α -DIO-eYFP (grey squares) injected bilaterally into BLA. In these animals, CeM-projecting BLA neurons express NpHR-eYFP or eYFP, respectively. **d**, Confocal image of

a representative CeM injection and NpHR-eYFP-expressing cells bodies in the BLA. **e**, Optical fibre tip placements over BLA from both hemispheres in animals injected with AAV₅-EF1 α -DIO-NpHR-eYFP in BLA and CAV-Cre in NAc (green circles) or CeM (red diamonds), or AAV₅-EF1 α -DIO-eYFP in BLA and CAV-Cre in NAc/CeM (grey squares). Horizontal lines represent thickness of the implanted fibre (300 μ m). **f**, Representative confocal images of optic fibre placements over BLA from both hemispheres of an animal injected with CAV-Cre in NAc and AAV₅-EF1 α -DIO-NpHR-eYFP in BLA. Note NpHR-eYFP-expressing NAc projectors in the BLA. Each atlas diagram and confocal image in a–f represents an area of 1.5 mm \times 1.5 mm; anteroposterior stereotaxic coordinates relative to Bregma are specified to the left of each image.



Extended Data Figure 6 | Tone-evoked freezing behaviour following inhibition of CeM or NAc projectors during auditory fear conditioning. **a**, Experimental design. Mice were trained in an auditory fear conditioning paradigm, during which NAc or CeM projectors were selectively inhibited using a dual virus recombination approach (Fig. 3). On the day following conditioning, mice were exposed to eight presentations of the conditioned stimulus alone. They were tethered to a patch cable but no light was delivered.

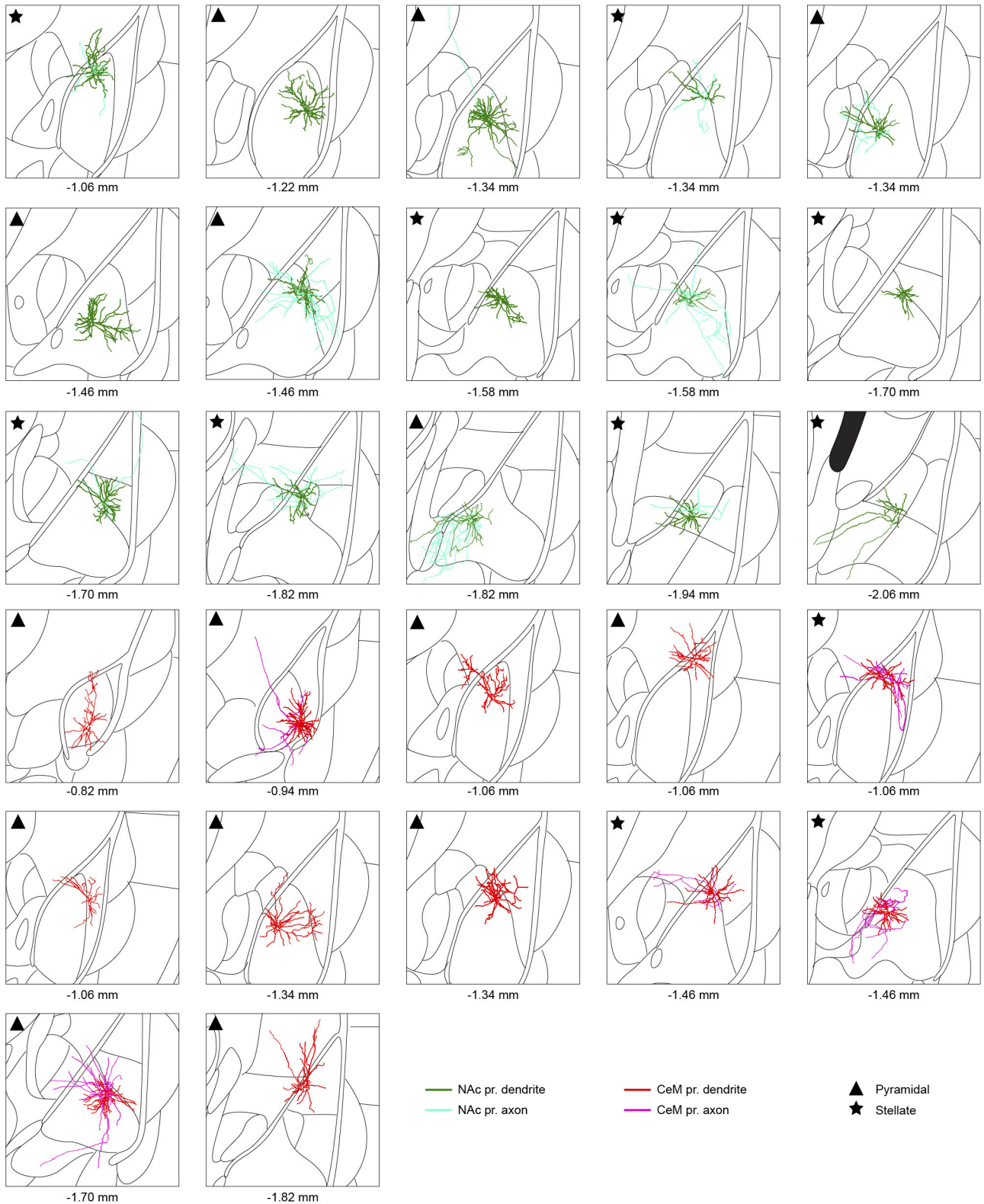
b, Time course of percentage freezing in mice expressing NpHR in NAc projectors (green circles), CeM projectors (red diamonds), or expressing eYFP in NAc or CeM projectors (grey squares) was quantified for each trial. **c**, There was no significant difference in freezing behaviour in response to the conditioned stimulus among the three groups of mice on test day (one-way ANOVA, $F_{2,38} = 2.010$, $P = 0.1488$). Results show mean and s.e.m.



Extended Data Figure 7 | Membrane properties of retrobead-positive NAc/CeM-projecting BLA neurons and rabies-virus-expressing BLA neurons.

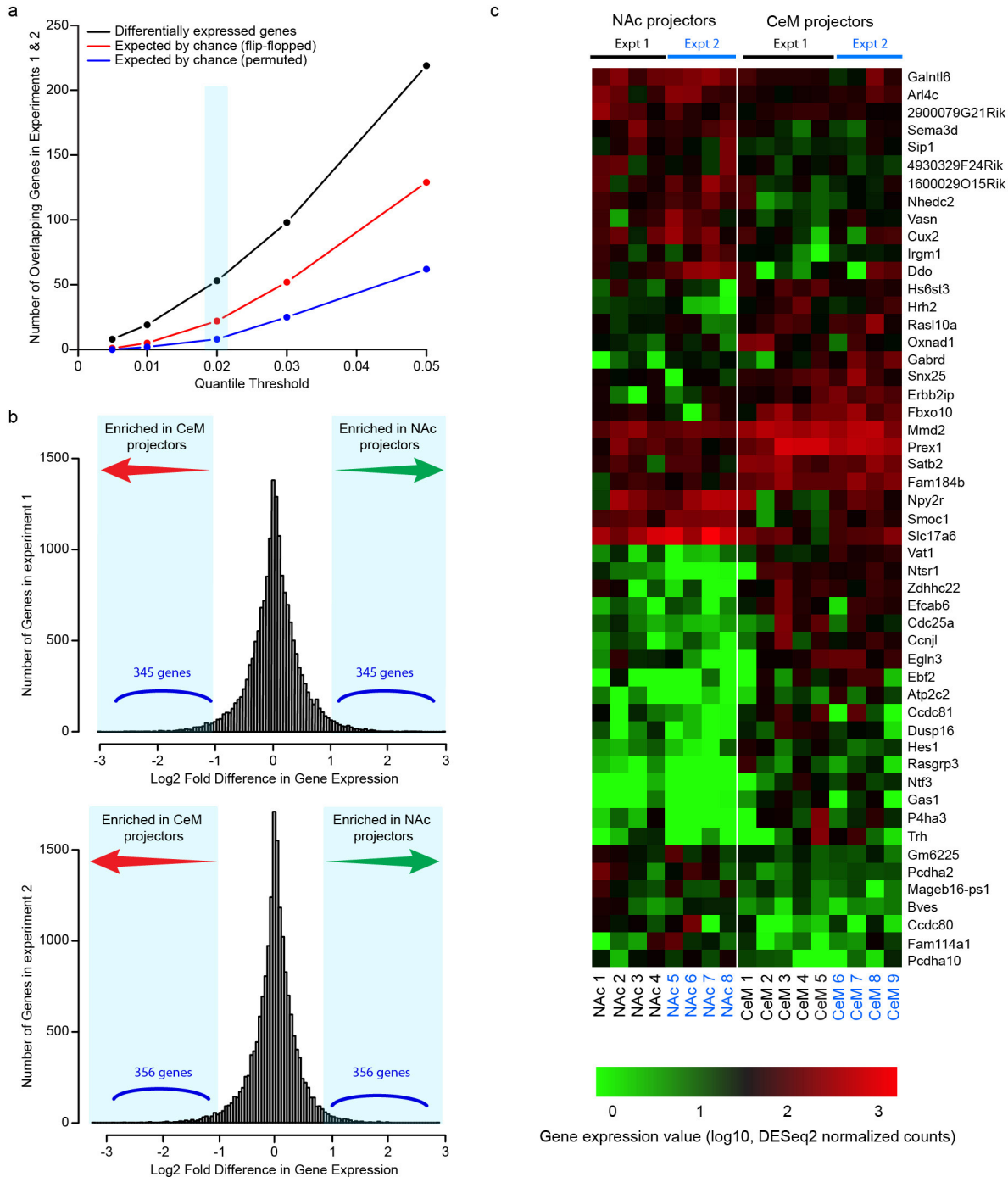
a, Access resistance, membrane resistance, and membrane capacitance were estimated from the current response of the cell to a 4 mV square voltage pulse using the Q-method³⁵. Access and membrane resistance as well as the membrane capacitance and membrane potential were not significantly different between the two populations (unpaired *t*-tests: $t_{20} = 0.788$, $P = 0.4400$; $t_{20} = 1.599$, $P = 0.1256$; $t_{20} = 1.847$, $P = 0.0796$; and $t_{18} = 0.2521$, $P = 0.8038$, respectively). The holding current corresponds to the current injected to clamp the cell at -70 mV. This value was not significantly different between NAc and CeM projectors (unpaired *t*-test, $t_{20} = 1.046$, $P = 0.3079$). **b**, Confocal image of a BLA–NAc projectors expressing ChR2–eYFP transduced by rabies virus (RV) and recorded *ex vivo* in whole-cell patch-clamp. The cell was filled with biocytin during recording and stained with streptavidin-CF405 (in grey). **c**, Current response to a 1-s blue light pulse in a cell expressing rabies virus, 5 days after injection. **d**, Five days after viral injection, rabies-virus-expressing

cells were able to respond with an action potential to every pulse of a 20 Hz light stimulation (5 ms pulses, top trace, blue line shows onset of light pulse). They also responded with an action potential to 250 pA, 5 ms current pulses injected at 20 Hz (middle trace). Rabies-virus-expressing cells also showed spontaneous post-synaptic excitatory and inhibitory currents (EPSCs and IPSCs, respectively) when clamped at -70 mV (bottom trace, 0 pA holding for this cell). **e**, Current/voltage curves are similar in retrobead (RB, grey circles, $n = 5$ cells) and rabies-virus-expressing cells (black circles, $n = 3$ cells). **f**, Average action potential for 11 retrobead-positive BLA–NAc projectors (grey) and six BLA–NAc projectors expressing rabies virus. **g**, Membrane properties of retrobead-positive versus rabies-virus-expressing neurons. None of the properties investigated were significantly altered in rabies-virus-expressing neurons (unpaired *t*-tests: access resistance, $t_{15} = 1.299$, $P = 0.2135$; membrane resistance, $t_{15} = 2.057$, $P = 0.0575$; membrane capacitance, $t_{15} = 1.215$, $P = 0.2430$; action potential threshold, $t_{15} = 0.0756$, $P = 0.9407$; holding current, $t_{16} = 1.002$, $P = 0.3314$). Results show mean and s.e.m.



Extended Data Figure 8 | Morphological reconstructions of individual BLA neurons projecting to NAc or CeM. Morphological reconstructions of all neurons used for Sholl analysis performed by Imaris software (Fig. 4i). Classification of each neuron as pyramidal or stellate is indicated in the top left

corner of each reconstructed neuron (triangle or star, respectively). Each atlas schematic represents 1.5 mm × 1.5 mm area and the corresponding anteroposterior stereotaxic coordinates (relative to Bregma) are shown below.



Extended Data Figure 9 | RNA-seq identification of candidate genes differentially expressed in NAc- and CeM-projecting BLA neurons.

a, Candidate differentially expressed genes were required to be enriched in only one group (either CeM or NAc projectors) in two independent experiments (NAc projectors collected from $n = 8$ mice; CeM projectors collected from $n = 9$ mice, total) at the indicated quantile fold-change threshold (light-blue column). One of the chance estimates ('flip-flopped', see Methods) is taken from genes that passed the quantile thresholds but were enriched in the opposite groups in the two experiments. Another chance estimate ('permuted', see Methods) is determined based on an analysis in which fold differences for each gene were permuted across genes within each of the two experiments before determining differential expression. A 0.02 quantile threshold was chosen to identify differentially expressed candidate genes in order to balance specificity and sensitivity, resulting in an estimated false discovery rate of 41.5%, calculated as the number expected by chance (flip-flopped) divided by

the number of differentially expressed genes (see Extended Data Fig. 9c for candidate gene list). In Fig. 4k, a 0.01 quantile threshold was chosen to identify a more conservative list of differentially expressed candidate genes at a lower false discovery rate of 26.2%. **b**, Distribution of differentially expressed genes between NAc and CeM projectors from RNA-seq experiments 1 and 2 (see Methods). Light-blue shaded areas represent the 2nd and 98th percentiles of the distributions. **c**, RNA-seq heat map showing normalized expression levels of differentially expressed genes in NAc- and CeM-projecting BLA neurons. Differentially expressed genes were required to be enriched in either NAc or CeM projectors in two independent experiments (samples used in experiment 1 are indicated in black text below the heat map; experiment 2 samples are indicated in blue text) at a 0.02 quantile threshold (Extended Data Fig. 9a). Each RNA-seq library was prepared from 35–60 manually sorted retrobead-labelled cells taken from the BLA.